

Manuscript version: Author's Accepted Manuscript

The version presented in WRAP is the author's accepted manuscript and may differ from the published version or Version of Record.

Persistent WRAP URL:

<http://wrap.warwick.ac.uk/130880>

How to cite:

Please refer to published version for the most recent bibliographic citation information. If a published version is known of, the repository item page linked to above, will contain details on accessing it.

Copyright and reuse:

The Warwick Research Archive Portal (WRAP) makes this work by researchers of the University of Warwick available open access under the following conditions.

© 2019 Elsevier. Licensed under the Creative Commons Attribution-NonCommercial-NoDerivatives 4.0 International <http://creativecommons.org/licenses/by-nc-nd/4.0/>.



Publisher's statement:

Please refer to the repository item page, publisher's statement section, for further information.

For more information, please contact the WRAP Team at: wrap@warwick.ac.uk.

Behaviour and design of stainless steel I-section columns in fire

Merih Kucukler^{a,*}, Zhe Xing^b, Leroy Gardner^b

^a*School of Engineering, University of Warwick, Coventry, CV4 7AL, UK*

^b*Department of Civil and Environmental Engineering, Imperial College London, London, SW7 2AZ, UK*

Abstract

The flexural buckling behaviour and design of stainless steel I-section columns at elevated temperatures are investigated in this paper. Finite element models able to accurately replicate the response of structural stainless steel columns in fire are created and validated. The models are then utilised to carry out extensive numerical parametric studies considering a broad range of stainless steel grades, cross-section geometries, slendernesses and elevated temperature levels. Using the results from the parametric studies, the safety and accuracy of existing design rules provided in the European structural steel fire design code EN 1993-1-2 for stainless steel columns in fire are assessed. It is observed that the existing design rules provide rather scattered and inaccurate ultimate strength predictions for stainless steel columns at elevated temperatures. For the purpose of establishing an accurate and practical means of designing stainless steel columns in fire, a new design approach, compatible with existing design rules in EN 1993-1-2, is proposed. The safety, accuracy and reliability of the proposed approach are illustrated for a wide range of cases against the results obtained through nonlinear finite element modelling. The proposed stainless steel column fire design rules are due to be incorporated into the upcoming version of the European steel fire design standard EN 1993-1-2.

Keywords: Fire; stainless steel; flexural buckling; finite element modelling; imperfections; local buckling; residual stresses

1. Introduction

Owing to the intrinsically different material response of stainless steel relative to carbon steel at elevated temperatures, stainless steel structural elements exhibit a significantly different response in fire relative to their carbon steel counterparts. However, the design provisions given in the current European structural fire design standard EN 1993-1-2 [1] for stainless steel structural elements in fire are largely based on those originally developed for structural elements made of carbon steel, leading to, in some areas, an inconsistent design treatment relative to their actual behaviour at elevated temperatures.

*Corresponding author

Email addresses: merih.kucukler@warwick.ac.uk (Merih Kucukler), zhe.xing16@imperial.ac.uk (Zhe Xing), leroy.gardner@imperial.ac.uk (Leroy Gardner)

To address the existing shortcomings, a number of research studies have recently been carried out to investigate the response of stainless steel elements in fire. Lopes et al. [2] performed numerical studies into the flexural buckling response of welded stainless steel I-section columns at elevated temperatures, observing the inaccuracy of the current design methods provided in EN 1993-1-2 [1]. However, since this study [2], revised elevated temperature stiffness and strength reduction factors for different stainless steel grades based on a greater number of experimental data have been developed and a new residual stress pattern for welded stainless steel I-sections [3] based on experimental measurements has been established. Gardner and Baddoo [4] conducted physical tests on stainless steel hollow section columns subjected to fire, whose results were utilised by Ng and Gardner [5, 6] to validate their numerical models; the validated models were employed to assess the accuracy of the design provisions provided in EN 1993-1-2 [1]. Uppfelt et al. [7], Tondini et al. [8], Liu et al. [9], Ding et al. [10] and Fan et al. [11] reported a series of physical experiments on stainless steel columns at elevated temperatures. Lopes et al. [12] carried out numerical parametric studies on stainless steel beam-columns in fire, also, along with [13], assessing the accuracy of current design provisions given by EN 1993-1-2 [1]. Although drawbacks to the current design provisions were highlighted, a new approach to the design of stainless steel members in fire has yet to be established and the full range of contributing parameters has yet to be systematically explored.

With the aim of establishing a consistent design approach for stainless steel structural elements in fire, a new design method for the flexural buckling assessment of stainless steel columns at elevated temperatures is proposed in this study. Finite element models able to replicate the physical response of stainless steel elements at elevated temperatures are firstly developed. Extensive parametric studies to furnish fundamental structural performance data are then performed. A broad range of elevated temperature levels, cross-section geometries, slendernesses and different stainless steel grades are taken into consideration. The accuracy and reliability of the proposed new design method, which is compatible with the existing methods provided for carbon steel columns in EN 1993-1-2 [1], are verified against the results from the nonlinear finite element modelling for all the considered cases.

2. Finite element modelling

In this section, finite element models able to mimic the response of stainless steel elements in fire are developed and validated against a series of experimental studies from the literature. The validated finite element models are employed in the following sections for the development and assessment of the proposed new design method.

2.1. Development of finite element models

The finite element models were created by means of the finite element analysis software Abaqus [14]. Denoted as S4R in the Abaqus element library, a four-noded, reduced integration, general purpose shell element able to consider transverse shear deformations and membrane strains was utilised to mesh all the finite element models. To capture elastic-plastic cross-section and overall member response influenced by both local and global instability effects, 16 elements were employed to model each flange and web plate. The number

of elements used along the length of the members was chosen such that the aspect ratios of the elements used in the web were approximately equal to unity for all the considered cases. Unless otherwise indicated, all the investigated columns had simply-supported end conditions, which were established by means of coupling constraints at the column ends.

Both local and global geometric imperfections were incorporated into the shell finite element models. The global imperfections were assumed to take the shape of a half-sine wave along the longitudinal axis and scaled to 1/1000 of the member length as shown in Fig. 1 (a). The local imperfections were directly defined through a series of repeated sinusoidal curves of half-wavelength L_w , in accordance with EN 1993-1-5 [15], as shown in Fig. 1 (b). The local web imperfection $e_{0,loc,web}$ was scaled to 1/200 of the web height h_w (i.e. $e_{0,loc,web} = h_w/200$) when the elastic buckling stress of the web-plate $\sigma_{cr,w}$ was lower than that of the flange plates $\sigma_{cr,f}$ (i.e. $\sigma_{cr,w} < \sigma_{cr,f}$), while the flange local imperfection $e_{0,loc,flange}$ was scaled to 1/50 of the half flange width b_f (i.e. $e_{0,loc,flange} = b_f/50$) when the flange plates had a lower elastic buckling stress $\sigma_{cr,f}$ than that of the web plate $\sigma_{cr,w}$ (i.e. $\sigma_{cr,w} < \sigma_{cr,f}$), as recommended in [15]; the local imperfection magnitude of the plate with the higher elastic buckling stress was defined such that a 90° angle at the web-flange junctions was retained.

To replicate the response of stainless steel columns in fire, the material stress-strain curve at room temperature was adjusted using the elevated temperature strength and stiffness reduction factors given in the Steel Construction Institute (SCI) Design Manual for Structural Stainless Steel [16], which are based on the results of extensive experimental measurements by [17–20]. It should be noted that in this study, grade 1.4301 austenitic, grade 1.4462 duplex and grade 1.4003 ferritic stainless steel grades were considered to generally represent the common grades of austenitic, duplex and ferritic stainless steel respectively. The full elevated temperature stress-strain curves were described using a two-stage Ramberg-Osgood material model [17, 21] as given by the following equations:

$$\begin{aligned} \epsilon &= \frac{\sigma}{E_\theta} + 0.002 \left(\frac{\sigma}{f_{p0.2,\theta}} \right)^{n_\theta} \quad \text{for } \sigma \leq f_{p0.2,\theta}, \\ \epsilon &= \frac{\sigma - f_{p0.2,\theta}}{E_{p0.2,\theta}} + \left(\epsilon_{u,\theta} - \epsilon_{p0.2,\theta} - \frac{f_{u,\theta} - f_{p0.2,\theta}}{E_{p0.2,\theta}} \right) \left(\frac{\sigma - f_{p0.2,\theta}}{f_{u,\theta} - f_{p0.2,\theta}} \right)^{m_\theta} + \epsilon_{p0.2,\theta} \\ &\quad \text{for } f_{p0.2,\theta} < \sigma \leq f_{u,\theta}, \end{aligned} \quad (1)$$

where σ and ϵ are the engineering stress and strain, E_θ is the Young's modulus at temperature θ , $f_{p0.2,\theta}$ is the 0.2% proof strength at temperature θ , $E_{p0.2,\theta}$ is the tangent modulus at $f_{p0.2,\theta}$, and $f_{u,\theta}$ is the ultimate strength at temperature θ . In eq. (1), n_θ and m_θ are the exponents defining the nonlinearity of the stress-strain curve, while $\epsilon_{0.2,\theta}$ is the total strain corresponding to $f_{p0.2,\theta}$. Note that the engineering stress-strain relationship given by eq. (1) was transformed into a true stress-strain relationship for input into the finite element models. The elevated temperature strengths $f_{p0.2,\theta}$ and $f_{u,\theta}$ were determined by multiplying the 0.2% proof strength reduction factor $k_{p0.2,\theta}$ and the ultimate strength reduction factor $k_{u,\theta}$ given in the SCI Design Manual for Structural Stainless Steel [16, 17] by the room temperature 0.2% proof strength f_y and ultimate strength f_u values, respectively. The room

temperature strengths, i.e. f_y and f_u , were taken as those proposed in [22] for hot-finished stainless steel plates. The elevated temperature ultimate strains ϵ_θ were determined using the following expression for austenitic and duplex stainless steel:

$$\epsilon_{u,\theta} = k_{\epsilon u,\theta} \left(1 - \frac{f_y}{f_u} \right) \quad (2)$$

and the following equation for ferritic stainless steel:

$$\epsilon_{u,\theta} = 0.6 k_{\epsilon u,\theta} \left(1 - \frac{f_y}{f_u} \right) \quad (3)$$

in which, $k_{\epsilon u,\theta}$ is the elevated temperature ultimate strain reduction factor taken from [16]. The elasticity modulus E_θ at temperature θ was calculated by multiplying the elasticity modulus reduction factor $k_{E,\theta}$ provided in [16] by the room temperature Young's modulus E taken as 200 GPa, i.e. $E_\theta = k_{E,\theta} E$. In accordance with the recommendations of the SCI Design Manual for Structural Stainless Steel [16], the values for the exponent n_θ used in eq. (1) were taken equal to the values recommended for room temperature in [22], while the m_θ values were determined using the expression below [23]:

$$m_\theta = \frac{\ln \left[\frac{\epsilon_{u,\theta} - \epsilon_{p0.2,\theta} (f_{u,\theta} - f_{p0.2,\theta}) / E_{p0.2,\theta}}{0.02 - \epsilon_{p0.2,\theta} (f_{2,\theta} - f_{p0.2,\theta}) / E_{p0.2,\theta}} \right]}{\ln \left(\frac{f_{u,\theta} - f_{p0.2,\theta}}{f_{2,\theta} - f_{p0.2,\theta}} \right)} \quad \text{but} \quad 1.50 \leq m_\theta \leq 5.00, \quad (4)$$

where $f_{2,\theta}$ is the strength at 2% total strain at temperature θ , determined by multiplying the 2% elevated temperature strength reduction factor $k_{2,\theta}$ given in [16] by the room temperature 0.2% proof strength f_y recommended by [22] for hot-finished stainless steel plates, i.e. $f_{2,\theta} = k_{2,\theta} f_y$. The use of m_θ determined from eq. (4) within eq. (1) ensures that the material stress-strain curves pass exactly through the defined $f_{p0.2,\theta}$, $f_{2,\theta}$ and $f_{u,\theta}$ strengths at the corresponding 0.2% proof strain, 2% total strain and ultimate strain values. Adopting eq. (1) in conjunction with the elevated temperature material property reduction factors provided in [16], the material stress-strain curves for the typical considered grades austenitic, duplex and ferritic stainless steel for different temperature levels are shown Fig. 2, in addition to those of carbon steel. Note that the carbon steel stress-strain curves were determined on the basis of the reduction factors and stress-strain model provided in EN 1993-1-2 [1]. As can be seen from Fig. 2, the elevated temperature stress-strain response of stainless steel is significantly different from that of carbon steel, and there is significant variation between different types of stainless steel.

The elevated temperature reduction factors $k_{E,\theta}$, $k_{p0.2,\theta}$, $k_{2,\theta}$ (see Fig. 3 (a)) adopted in this study, which were taken from [16], are shown in Fig. 3 for the considered grades of (b) austenitic, (c) duplex and (d) ferritic stainless steel; those for carbon steel [1] are also shown for comparison in Fig. 3 (e). As can be seen from the figure, the strength reduction is more severe than the Young's modulus reduction for stainless steel in fire. By contrast, the Young's modulus reduction is more severe relative to the strength reduction for carbon

steel at elevated temperatures. It is also worth noting that stainless steel generally exhibits better Young's modulus and strength retention relative to carbon steel in fire.

In this study, it was assumed that the considered stainless steel I-section columns were fabricated by the welding of individual hot-finished stainless steel plates. Thus, the residual stress pattern put forward by Yuan et al. [3] and shown in Fig. 4, based on measurements made on a series of stainless steel welded I-sections, was used to define the residual stresses in the finite element models. As can be seen in Fig. 4, the maximum tensile residual stresses in the flanges σ_{ft} and web σ_{wt} are taken as 80% of the 0.2% proof stress f_y for austenitic stainless steel members and 60 % of the 0.2% proof stress f_y for duplex and ferritic stainless steel members, i.e. $\sigma_{ft} = \sigma_{wt} = 0.8f_y$ for austenitic stainless steel and $\sigma_{ft} = \sigma_{wt} = 0.6f_y$ for duplex and ferritic stainless steel members. The maximum compressive residual stresses within the flanges and web were determined on the basis of axial force equilibrium as described in [3]. The residual stress pattern shown in Fig. 4 was incorporated into the FE models in a step-wise fashion by defining constant values (taken at the middle of each element) of residual stress at the element integration points at room temperature. Since the residual stresses were applied at room temperature, their magnitudes reduced with the development of thermal strains when the models were heated up.

The finite element models were analysed isothermally using the following steps: (i) application of the residual stresses σ_{res} shown in Fig. 4 in conjunction with the corresponding residual plastic strains $\epsilon_{res,pl}$ at room temperature, with the latter determined considering the Ramberg-Osgood material model given by eq. (1) and using the expression below:

$$\epsilon_{res,pl} = \frac{\sigma_{res}}{E} + 0.002 \left(\frac{\sigma_{res}}{f_y} \right)^n - \epsilon_{res,el} = 0.002 \left(\frac{\sigma_{res}}{f_y} \right)^n, \quad (5)$$

where $\epsilon_{res,el} = \sigma_{res}/E$ is the elastic component of the total strain resulting from the corresponding residual stress [24], (ii) incremental application of a uniform temperature increase to the models from room temperature to a predefined temperature value θ leading to the development of thermal strains in the models and the modification of their material response as shown in Fig. 2 and finally, (iii) application of the loading to the finite element models at the designated elevated temperature θ value. In the last step, the modified Riks method [25, 26] was used so as to trace the full load-displacement response, while the first two steps were finalised only after reaching self-equilibrium in the models. Since the finite element models were analysed isothermally, the peak loads were taken directly as the ultimate load carrying capacities of the stainless steel columns at the prescribed elevated temperature levels. A finite element model of a typical column is shown in Fig. 5.

2.2. Validation of finite element models

Validation of the adopted finite element modelling approach is presented in this subsection. Validation was carried out against the results of fire tests performed on stainless steel box section columns [4, 8, 20], stainless steel I-section columns with end restraint [9] and carbon steel I-section columns [27], as described in the following three sub-sections. Note that the general finite element modelling approach adopted in this study was also validated

in Kucukler et al. [28] and Bu and Gardner [29] against experiments performed on stainless steel I-section elements at room temperature

2.2.1. Validation against experiments on stainless steel box section members

The experiments carried out by Gardner and Baddoo [4] and Ala-Outinen and Oksanen [20] on a series of austenitic stainless steel box section columns and those performed by Tondini et al. [8] on three ferritic stainless steel box-section columns were first utilised to validate the finite element modelling approach adopted in this paper. In all the considered studies [4, 8, 20], the tests were carried out anisothermally, whereby a certain axial load was first applied to the specimens and then the temperature was increased until failure; the temperature level at which the column fails is referred to as the critical temperature θ_{cr} . The geometrical and material properties of the specimens and the measured temperature-time relationships reported in [4, 8, 20] were included in the finite element models. Unlike the tests of [4, 20], the temperature of the specimens was not measured during the experiments carried out by Tondini et al. [8]; only the air temperature within the furnace was provided. Thus, for the purpose of estimating the temperature development within the specimens of [8], heat transfer analyses were performed herein using the reported average furnace air temperature versus time relationships. In these analyses, specific heat was determined from the expression given in EN 1993-1-2 [1]; the convective heat transfer coefficient α_c and emissivity ϵ_m were taken as 25 W/mm²K and 0.4 in accordance with [1] respectively (i.e. $\alpha_c=25$ W/mm²K and $\epsilon_m = 0.4$). Comparisons between the critical temperature values obtained through the experiments $\theta_{cr,test}$ and finite element models $\theta_{cr,FE}$ in this study are shown in Table 1, where it can be seen that the agreement between the experimentally and numerically obtained critical temperature values is good. The conservative critical temperature predictions of the finite element models $\theta_{cr,FE}$ for the austenitic stainless steel columns are ascribed to the assumption of constant temperature through the thickness of the cross-sections, whereas the small overpredictions of the critical temperatures of the ferritic stainless steel columns are attributed to the underestimation of the temperature development within the specimens through the heat transfer analyses.

The temperature versus mid-height lateral deformation of a typical tested [4] and simulated austenitic stainless steel column - a 3.4 m long fixed ended RHS 150×100×6 column subjected to an axial load of 268 kN - is shown in Fig. 6, where a close agreement between the experimental and numerical results can be seen. Similarly, the temperature versus axial deformation responses of the three ferritic stainless steel columns reported in [8] are compared in Fig. 7, indicating that the finite element models are able to replicate the experimental behaviour.

2.2.2. Validation against experiments carried out on restrained stainless steel I-section members

Liu et al. [9] reported a number of fire tests on restrained austenitic stainless steel welded I-section columns, the results of which are utilised to validate further the developed finite element models. The experiments were carried out anisothermally whereby the specimens were first subjected to a prescribed level of axial compression and then heated up until

failure. The specimens were axially and/or rotationally restrained to observe the influence of end restraints on the fire resistance of stainless steel columns. The material properties and initial geometric imperfection amplitudes reported by [9] were adopted in the FE models. The corresponding surface temperature versus time relationships measured in [9] for the specimens were utilised in the finite element element simulations. The axial and rotational restraints were simulated by linear elastic translational and rotational springs within the models with an axial stiffness of $k_{\Delta} = 7390 \text{ kN/m}$ and a rotational stiffness of $k_{\phi} = 1.88 \times 10^4 \text{ kNm/rad}$ following the recommendations of [9]. Fig. 9 shows comparisons between the experimental and numerical axial deformation versus temperature paths. As can be seen from the figure, the agreement between the experimental and numerical axial deformation versus temperature paths is good, indicating that the finite element models are able to replicate the response of stainless steel I-section columns in fire.

2.2.3. Validation against experiments carried out on carbon steel I-section members

Finally, the models are also validated against the fire tests performed on carbon steel I-sections by Pauli et al. [27]. Pauli et al. [27] carried out a series of tests on pin-ended columns made of grade S 355 carbon steel with a European HEA 100 cross-section undergoing major and minor axis flexural buckling at a range of elevated temperature levels; the results of these tests are utilised herein for the validation of the finite element models. The experiments were conducted isothermally, whereby the columns were first heated to a specified temperature level and then loaded until failure. The measured geometrical properties, elevated temperature material properties and mean values of local and global geometrical imperfections of the specimens reported by Pauli et al. [27] were incorporated into the finite element models created herein. In Fig. 8, the load versus end-shortening paths of the specimens undergoing major and minor axis buckling at elevated temperature levels of 400 °C, 550 °C and 700 °C, as well as at room temperature, obtained from the experiments and the finite element modelling approach adopted in this study are compared. As can be seen from the figure, the correlation between the experimental and numerical load-displacement paths is good. Additionally, the ultimate axial load carrying capacities of the specimens determined by Pauli et al. [27] $N_{u,test}$ and those obtained from the finite element developed herein $N_{u,FE}$ are also compared Table 2. The ultimate loads determined by the experiments and finite element models are in close agreement, indicating that the finite element models developed in this study are capable of replicating the flexural buckling response of steel I-section columns at elevated temperatures.

3. Local buckling assessment of stainless steel columns in fire

Prior to the development of a design method for the flexural buckling assessment of stainless steel columns in fire, the effective width formulations developed by Xing et al. [30] for the local buckling assessment of stainless steel plates in fire are briefly introduced in this section. These formulations will be used in conjunction with the proposed flexural buckling assessment equations for the determination of the ultimate strengths of stainless steel columns undergoing interactive local and global buckling in fire in Section 5.

3.1. New effective width formulations for local buckling assessment of stainless steel elements in fire

Currently, in EN 1993-1-2 [1], while the elevated temperature strength at 2% total strain $f_{2,\theta}$ is used for the determination of the ultimate strengths of Class 1,2 and 3 cross-sections, the elevated temperature 0.2% proof stress $f_{p0.2,\theta}$ is used for Class 4 sections. A number of studies [31, 32] have pointed out the inconsistency and inaccuracy of the use of two different reference strengths (i.e. $f_{2,\theta}$ and $f_{p0.2,\theta}$) for different cross-section classes. In line with these studies, Xing et al. [30] developed a design proposal for stainless steel in which $f_{2,\theta}$ is used as the basis for the determination of the resistances of all four classes of cross-sections.

3.1.1. Formulations based on elevated temperature strength at 2% total strain $f_{2,\theta}$

Adopting the effective width concept provided in EN 1993-1-5 [15], Xing et al. [30] developed the following equations for the determination of the effective widths for austenitic stainless steel internal compression elements using $f_{2,\theta}$ as the reference strength:

$$\rho = \begin{cases} \rho = 1.0 & \text{for } \bar{\lambda}_{p,\theta} \leq \bar{\lambda}_{p,\theta,0} \\ \frac{0.54}{(\bar{\lambda}_{p,\theta}/\xi_\theta)^{0.75}} - \frac{0.015(3+\psi)}{(\bar{\lambda}_{p,\theta}/\xi_\theta)^{1.5}} & \text{for } \bar{\lambda}_{p,\theta} > \bar{\lambda}_{p,\theta,0}, \end{cases} \quad (6)$$

in which

$$\xi_\theta = \sqrt{\frac{k_{2,\theta}}{k_{E,\theta}}} \quad (7)$$

and

$$\bar{\lambda}_{p,\theta,0} = \left(0.27 + \sqrt{0.0279 - 0.015\psi}\right)^{1.33} \sqrt{\xi_\theta}. \quad (8)$$

The following equations were developed [30] for the determination of the effective widths of duplex and ferritic stainless steel internal compression elements:

$$\rho = \begin{cases} \rho = 1.0 & \text{for } \bar{\lambda}_{p,\theta} \leq \bar{\lambda}_{p,\theta,0} \\ \frac{0.6}{(\bar{\lambda}_{p,\theta}/\xi_\theta)^{0.75}} - \frac{0.015(3+\psi)}{(\bar{\lambda}_{p,\theta}/\xi_\theta)^{1.5}} & \text{for } \bar{\lambda}_{p,\theta} > \bar{\lambda}_{p,\theta,0} \end{cases} \quad (9)$$

in which

$$\bar{\lambda}_{p,\theta,0} = \left(0.3 + \sqrt{0.045 - 0.015\psi}\right)^{1.33} \sqrt{\xi_\theta}. \quad (10)$$

For austenitic stainless steel outstand compression elements, the following expressions were developed [30]:

$$\rho = \begin{cases} \rho = 1.0 & \text{for } \bar{\lambda}_{p,\theta} \leq \bar{\lambda}_{p,\theta,0} \\ \frac{0.6}{(\bar{\lambda}_{p,\theta}/\xi_\theta)^{0.6}} - \frac{0.075}{(\bar{\lambda}_{p,\theta}/\xi_\theta)^{1.2}} & \text{for } \bar{\lambda}_{p,\theta} > \bar{\lambda}_{p,\theta,0} \end{cases} \quad (11)$$

where

$$\bar{\lambda}_{p,\theta,0} = 0.237\sqrt{\xi_\theta} \quad (12)$$

and for the duplex and ferritic stainless steel plates, the expressions below were put forward [30]:

$$\rho = \begin{cases} 1.0 & \text{for } \bar{\lambda}_{p,\theta} \leq \bar{\lambda}_{p,\theta,0} \\ \frac{0.67}{(\bar{\lambda}_{p,\theta}/\xi_\theta)^{0.6}} - \frac{0.075}{(\bar{\lambda}_{p,\theta}/\xi_\theta)^{1.2}} & \text{for } \bar{\lambda}_{p,\theta} > \bar{\lambda}_{p,\theta,0} \end{cases} \quad (13)$$

where

$$\bar{\lambda}_{p,\theta,0} = 0.344\sqrt{\xi_\theta} \quad (14)$$

In eq. (6), eq. (9), eq. (11) and eq. (13), ρ is the reduction factor for local plate buckling, which is multiplied by the full width of a plate b to give its effective width b_{eff} (i.e. $b_{eff} = \rho b$), ψ is the ratio between the stresses at the edges of the plate as described in EN 1993-1-5 [15], $\bar{\lambda}_{p,\theta,0}$ is the threshold plate slenderness below which $\rho = 1.0$ and $\bar{\lambda}_{p,\theta}$ is the elevated temperature plate slenderness given by:

$$\bar{\lambda}_{p,\theta} = \xi_\theta \sqrt{\frac{f_y}{f_{cr}}} \quad \text{with} \quad \xi_\theta = \sqrt{\frac{k_{2,\theta}}{k_{E,\theta}}} \quad (15)$$

where f_y is the room temperature 0.2% proof strength and f_{cr} is the elastic critical buckling stress of the plate at room temperature calculated as follows

$$f_{cr} = k_\sigma \frac{\pi^2 E}{12(1 - \nu^2)} \left(\frac{t}{b}\right)^2 \quad (16)$$

in which k_σ is the buckling factor determined for the corresponding stress distribution and boundary conditions of the compression element following the guidance provided in EN 1993-1-5 [33], and b and t are the plate width and thickness, respectively.

In the proposals of [30], if $\bar{\lambda}_{p,\theta} \leq \bar{\lambda}_{p,\theta,0}$ for all compression elements in a cross-section, then the cross-section is classified as ‘non-slender’, while if one or more compression elements have $\bar{\lambda}_{p,\theta} > \bar{\lambda}_{p,\theta,0}$, then the cross-section is classified as ‘slender’. The ultimate elevated temperature axial force resistance of a cross-section $N_{fi,\theta,Rd}$ is determined using the following equations:

$$N_{fi,\theta,Rd} = \begin{cases} \frac{Ak_{2,\theta}f_y}{\gamma_{M,fi}} & \text{for non-slender sections} \\ \frac{A_{eff}k_{2,\theta}f_y}{\gamma_{M,fi}} & \text{for slender sections} \end{cases} \quad (17)$$

where A is the full cross-section area, A_{eff} is the effective cross-section area and $\gamma_{M,fi}$ is the partial safety factor equal to unity. It is worth mentioning that in line with the proposals made by Xing et al. [30], Couto et al. [32] also pointed out the practicality and higher accuracy of adopting two cross-section classes for carbon steel elements in fire with $f_{2,\theta}$ as the reference strength.

4. EN 1993-1-2 rules for flexural buckling assessment of stainless steel columns in fire

As previously indicated, in spite of the different material response of stainless steel relative to carbon steel at elevated temperatures, EN 1993-1-2 [33] provides the same form of column buckling design rules for both carbon steel and stainless steel columns in fire. Adopting the traditional Perry-Robertson concept [34, 35] used in EN 1993-1-1 [33] for room temperature design, the European structural fire design code EN 1993-1-2 [1] provides the following expressions for the assessment of the flexural buckling resistance of stainless steel columns at a uniform elevated temperature θ :

$$\begin{aligned} N_{b,fi,t,Rd} &= \frac{\chi_{fi} A k_{2,\theta} f_y}{\gamma_{M,fi}} \quad \text{for Class 1, 2 and 3 sections,} \\ N_{b,fi,t,Rd} &= \frac{\chi_{fi} A_{eff} k_{p0.2,\theta} f_y}{\gamma_{M,fi}} \quad \text{for Class 4 sections,} \end{aligned} \quad (18)$$

where $N_{b,fi,t,Rd}$ is the design buckling resistance at time t of a compression member, $\gamma_{M,fi}$ is the partial safety factor taken equal to 1.0, f_y is the 0.2% proof strength at room temperature, A is the cross-sectional area for Class 1, 2 and 3 sections based on the cross-section classification rules provided in EN 1993-1-4 [36], A_{eff} is the effective cross-sectional area for Class 4 sections calculated adopting the room temperature effective width calculation rules given in [36] with $\epsilon = 0.85\sqrt{(235/f_y)/(E/210000)}$ and χ_{fi} is the elevated temperature column buckling reduction factor calculated as

$$\chi_{fi} = \frac{1}{\phi_\theta + \sqrt{\phi_\theta^2 - \bar{\lambda}_\theta^2}} \quad \text{where} \quad \phi_\theta = 0.5 \left[1 + \eta_\theta + \bar{\lambda}_\theta^2 \right], \quad (19)$$

in which η_θ is the generalised imperfection factor expressed as

$$\eta_\theta = \alpha \bar{\lambda}_\theta \quad \text{with} \quad \alpha = 0.65 \sqrt{235/f_y}. \quad (20)$$

Note that the generalised imperfection factor η_θ is the primary parameter determining the shape of a buckling curve. In eq. (19) and eq. (20), $\bar{\lambda}_\theta$ is the non-dimensional slenderness at temperature θ calculated using the following expression:

$$\bar{\lambda}_\theta = \sqrt{\frac{A f_y}{N_{cr}}} \sqrt{\frac{k_{2,\theta}}{k_{E,\theta}}} = \bar{\lambda} \sqrt{\frac{k_{2,\theta}}{k_{E,\theta}}} \quad \text{for Class 1, 2 and 3 sections,} \quad (21)$$

$$\bar{\lambda}_\theta = \sqrt{\frac{A_{eff} f_y}{N_{cr}}} \sqrt{\frac{k_{2,\theta}}{k_{E,\theta}}} = \bar{\lambda} \sqrt{\frac{k_{2,\theta}}{k_{E,\theta}}} \quad \text{for Class 4 sections,} \quad (22)$$

where N_{cr} and $\bar{\lambda}$ are the elastic critical buckling load and non-dimensional slenderness at room temperature, respectively.

In Fig. 10, the existing EN 1993-1-2 [1] rules for the flexural buckling assessment of stainless steel columns are compared against the ultimate strengths predicted by the geometrically and materially nonlinear analyses with imperfections (GMNIA) of the shell finite element models of welded columns with cross-sections having the shape of an HEB 300 profile without the presence of the fillets, considering austenitic, duplex and ferritic stainless steel grades and various temperature levels and non-dimensional slenderness values. Note that the GMNIA results are assumed as the benchmark data. As can be seen from Fig. 10, the current EN 1993-1-2 [1] rules provide a single buckling curve leading to flexural buckling strength predictions on the unsafe side for the majority of columns regardless of the stainless steel grade, indicating that improvements to the current design rules are necessary. It is important to note that the overpredictions of resistance of EN 1993-1-2 increase with increasing temperature level. Similar observations were also made in [2] and are confirmed further in Section 5 for a wider range of stainless steel columns with different cross-sections and proportions.

5. Development of new flexural buckling rules for stainless steel columns in fire

In this section, flexural buckling curves for the design of stainless steel columns at elevated temperatures are developed. A new set of buckling curves, based on the elevated temperature strength at 2% total strain $f_{2,\theta}$, are calibrated against results from nonlinear shell finite element modelling considering a wide range of slenderness values, cross-section geometries and elevated temperature values for the three primary stainless steel grades (i.e. austenitic, duplex and ferritic). Use of the elevated temperature strength at 2% total strain $f_{2,\theta}$ in the proposed method is consistent with the existing design rules for carbon steel columns provided in EN 1993-1-2 [1]. It should be noted that all the GMNIA carried out in this section were performed isothermally. Even though isothermal simulations do not follow the sequence typically observed in real fire scenarios, such simulations have been widely adopted in previous studies, including in the development of the new local buckling and lateral-torsional buckling design equations that will be incorporated into the upcoming version of EN 1993-1-2, as reported in Couto et al. [31] and Couto et al. [37], respectively. The isothermal simulations provide a reliable means of assessing the elevated temperature response of steel members and are well suited to the development of design guidance since they enable the ultimate load of a member at a particular temperature to be directly obtained.

5.1. New proposal for the definition of the generalised imperfection factor η_θ

The European structural fire design code EN 1993-1-2 [1] adopts the Perry-Robertson concept [34, 35] for the fire design of columns, which is based on the second-order elastic analysis of a pin-ended column with a half-sine wave imperfection along its length scaled to a magnitude of \bar{e}_0 at mid-height as shown in Fig. 11. According to this concept, failure of a column is signified by first yield occurring at the extreme compressive fibre of the mid-height cross-section on the concave side of the member. The imperfection magnitude \bar{e}_0 , which is directly proportional to the column length, is calibrated such that it considers fully the adverse influence of the development and spread of plasticity, residual stresses and

geometrical imperfections on the ultimate load carrying capacity of a column; \bar{e}_0 is thus also referred to as an ‘equivalent imperfection’ in the literature.

The derivation of the column buckling equations in EN 1993-1-2 [1] is based on the attainment of first yield (though taken as the strength at 2% strain) at the mid-height section of a steel column in fire shown in Fig. 11 and using the equation below:

$$\frac{N_{Ed}}{Ak_{2,\theta}f_y} + \frac{N_{Ed}\bar{e}_0}{W_{el}k_{2,\theta}f_y} \frac{1}{1 - N_{Ed}/(k_{E,\theta}N_{cr})} = 1.0, \quad (23)$$

where W_{el} is the elastic section modulus and N_{cr} is the elastic buckling load relevant to the axis of buckling. Defining the column buckling reduction factor in fire χ_{fi} and elevated temperature non-dimensional column buckling slenderness $\bar{\lambda}_\theta$ as:

$$\chi_{fi} = \frac{N_{Ed}}{Ak_{2,\theta}f_y} \quad \text{and} \quad \bar{\lambda}_\theta = \sqrt{\frac{Af_y}{N_{cr}}} \sqrt{\frac{k_{2,\theta}}{k_{E,\theta}}}, \quad (24)$$

eq. (23) can be expressed as follows:

$$\chi_{fi} + \chi_{fi} \frac{1}{1 - \chi_{fi}\bar{\lambda}_\theta^2} \eta_\theta = 1.0, \quad (25)$$

where the generalised imperfection factor η_θ is equal to:

$$\eta_\theta = \frac{A\bar{e}_0}{W_{el}}. \quad (26)$$

Solving eq. (24) for χ_{fi} gives the expression below provided in EN 1993-1-2 for the determination of the column buckling reduction factor in fire χ_{fi} , which is also given by eq. (19):

$$\chi_{fi} = \frac{1}{\phi_\theta + \sqrt{\phi_\theta^2 - \bar{\lambda}_\theta^2}} \quad \text{where} \quad \phi_\theta = 0.5 \left[1 + \eta_\theta + \bar{\lambda}_\theta^2 \right] \quad (27)$$

In the development of the EN 1993-1-2 [1] column buckling rules, considering the actual elastic-plastic response of an imperfect steel column, the calibration of the Perry-Robertson equation was carried out such that the expression for the generalised imperfection factor η_θ given by eq. (26) was replaced by the expression given below

$$\eta_\theta = \alpha \bar{\lambda}_\theta. \quad (28)$$

Using eq. (26) and eq. (28), the equivalent imperfection \bar{e}_0 of the column can be expressed as

$$\bar{e}_0 = \alpha \frac{W_{el}}{A} \bar{\lambda}_\theta = \alpha \frac{W_{el}}{A} \bar{\lambda}_\theta \sqrt{\frac{k_{2,\theta}}{k_{E,\theta}}}. \quad (29)$$

Considering a column with a welded section having cross-section properties the same as an HEB 300 section and buckling about the minor axis, the ratio of the equivalent imperfection \bar{e}_0 to the column length L , i.e. \bar{e}_0/L , calculated according to EN 1993-1-2 [1] as given by eq. (29), is shown for a range of elevated temperature values in Fig. 12 for austenitic stainless steel and carbon steel columns. As can be seen from the figure, the \bar{e}_0/L ratios change with the elevated temperature level – Fig. 12 (a) shows that for austenitic stainless steel, the higher the temperature, the lower the \bar{e}_0/L ratio; the same trend is also observed for duplex and ferritic stainless steel grades. On the other hand, for the case of carbon steel, the \bar{e}_0/L ratios assume greater values with increasing temperature, as can be seen from Fig. 12 (b). Clearly, imperfection magnitudes changing with temperature (reducing in size for stainless steel and increasing in size for carbon steel at higher temperatures) does not reflect the physical reality of the situation; this shortcoming is addressed below.

The dependency of \bar{e}_0/L on temperature results from the equivalent imperfection \bar{e}_0 being a function of $\xi_\theta = \sqrt{k_{2,\theta}/k_{E,\theta}}$, as can be seen from eq. (29). Fig. 13 shows that $\xi_\theta = \sqrt{k_{2,\theta}/k_{E,\theta}}$ decreases with increasing temperature for stainless steels, indicating that the strength reduction is more severe than the stiffness reduction at elevated temperatures, while the opposite is the case for carbon steel. Thus, whereas the ratio of the equivalent imperfection to the column length \bar{e}_0/L decreases with increasing temperature for stainless steel, it increases at higher temperature levels for carbon steel, leading to a situation where the EN 1993-1-2 [1] design predictions become unconservative for stainless steel columns as shown in Fig. 10, but are acceptable for carbon steel columns as illustrated in [38].

Since the equivalent imperfection \bar{e}_0 should not logically be dependent upon temperature, or have the opposite trend with temperature for stainless steel and carbon steel, this study recommends the following expression of the generalised imperfection factor:

$$\eta_\theta^* = \alpha \bar{\lambda}_\theta / \xi_\theta \quad (30)$$

whereby \bar{e}_0 can be expressed as

$$\bar{e}_0 = \alpha \frac{W_{el}}{A} \bar{\lambda}_\theta / \xi_\theta = \alpha \frac{W_{el}}{A} \bar{\lambda} \sqrt{\frac{k_{2,\theta}}{k_{E,\theta}}} / \sqrt{\frac{k_{2,\theta}}{k_{E,\theta}}} = \alpha \frac{W_{el}}{A} \bar{\lambda}, \quad (31)$$

thus leading to a constant value of \bar{e}_0/L regardless of the temperature level as shown below:

$$\bar{e}_0/L = \alpha \frac{W_{el}}{A} \bar{\lambda} / L = \alpha \frac{W_{el}}{A} \left(\frac{L}{i} \sqrt{\frac{f_y}{\pi^2 E}} \right) / L = \alpha \frac{W_{el}}{A} \left(\frac{1}{i} \sqrt{\frac{f_y}{\pi^2 E}} \right), \quad (32)$$

where i is the radius of gyration for the axis about which the buckling occurs. Adopting the newly proposed generalised imperfection factor η_θ^* given by eq. (30), new flexural buckling curves are developed in the next subsection.

5.2. New design rules for flexural buckling assessment of stainless steel columns in fire

Similar to the cross-section design rules developed in [30], the elevated temperature strength at 2% total strain $f_{2,\theta}$ was adopted in the development of the new proposals for the

flexural buckling design of stainless steel columns in fire. The new proposals are based on the Perry-Robertson concept [34, 35] and are thus compatible with the existing design rules in EN 1993-1-2 [1]. The accuracy of the new proposals is assessed against GMNIA results and the existing EN 1993-1-2 [1] rules considering a wide range of cases in Section 5.4.

5.2.1. New design expressions based on elevated temperature strength at 2% total strain $f_{2,\theta}$

Adopting the elevated temperature strength at 2% total strain $f_{2,\theta} = k_{2,\theta}f_y$, the following equations are proposed for the flexural buckling assessment of stainless steel columns in fire in this study:

$$\begin{aligned} N_{b,fi,t,Rd} &= \frac{\chi_{fi} A k_{2,\theta} f_y}{\gamma_{M,fi}} \quad \text{for non-slender sections,} \\ N_{b,fi,t,Rd} &= \frac{\chi_{fi} A_{eff} k_{2,\theta} f_y}{\gamma_{M,fi}} \quad \text{for slender sections,} \end{aligned} \quad (33)$$

in which

$$\chi_{fi} = \frac{1}{\phi_\theta + \sqrt{\phi_\theta^2 + \beta \bar{\lambda}_\theta^2}} \quad \text{where} \quad \phi_\theta = 0.5 \left[1 + \alpha \bar{\lambda}_\theta / \xi_\theta + \beta \bar{\lambda}_\theta^2 \right] \quad (34)$$

where α is the imperfection factor, β is the auxiliary coefficient, $\xi_\theta = \sqrt{k_{2,\theta}/k_{E,\theta}}$ is the elevated temperature strength-to-stiffness ratio reduction factor and $\bar{\lambda}_\theta$ is the elevated temperature non-dimensional slenderness calculated as

$$\begin{aligned} \bar{\lambda}_\theta &= \bar{\lambda} \xi_\theta = \sqrt{\frac{A f_y}{N_{cr}}} \sqrt{\frac{k_{2,\theta}}{k_{E,\theta}}} \quad \text{for non-slender sections} \\ \bar{\lambda}_\theta &= \bar{\lambda} \xi_\theta = \sqrt{\frac{A_{eff} f_y}{N_{cr}}} \sqrt{\frac{k_{2,\theta}}{k_{E,\theta}}} \quad \text{for slender sections.} \end{aligned} \quad (35)$$

Note that A_{eff} is determined using the expressions provided in Subsection 3.1.1, classifying a column cross-section as either ‘non-slender’ or ‘slender’ on the basis of the given procedure.

5.3. Calibration of the proposed design rules

Expressing eq. (34) in terms of the generalised imperfection factor $\eta_\theta^* = \alpha \bar{\lambda}_\theta / \xi_\theta$, and taking the ratio of the ultimate strength determined by the GMNIA to the ultimate axial resistance of the cross-section as χ_{FE} , (i.e. $\chi_{FE} = N_{Ed,max,FE} / (A k_{2,\theta} f_y)$ or $\chi_{FE} = N_{Ed,max,FE} / (A_{eff} k_{2,\theta} f_y)$ depending on whether the cross-section is slender or non-slender according to [30]), the numerical generalised imperfection factors $\eta_{\theta,FE}^*$ can be determined by:

$$\eta_{\theta,FE}^* = \left(\frac{1}{\chi_{FE}} - 1 \right) \left(1 - \beta \chi_{FE} \bar{\lambda}_\theta^2 \right). \quad (36)$$

In this study, η_θ^* given in eq. (30), with $\xi_\theta = \sqrt{k_{2,\theta}/k_{E,\theta}}$, was calibrated against the $\eta_{\theta,FE}^*$ values obtained from GMNIA through eq. (36), as shown in Fig. 14 for a series of austenitic

stainless steel columns undergoing major axis buckling at various temperature levels. In the figure, the considered range of elevated temperature non-dimensional slenderness of the columns $\bar{\lambda}_\theta$ may be seen to be between 0.1 and 2.0, while for the cross-sections, seven welded I-section profiles with the same properties as those of European HE and IPE sections, whose proportions ranged between the values given in Table 3, were considered. As can be seen from Fig. 14, incorporation of the elevated temperature strength-to-stiffness ratio reduction factor ξ_θ within η_θ^* captures the requirement for larger generalised imperfection factor values $\eta_{\theta,FE}^*$ for higher temperature levels.

The same calibration procedure was also followed for austenitic columns undergoing minor axis buckling, as well as duplex and ferritic stainless steel columns buckling about both axes. Seven cross-section profiles were considered for each of the austenitic and ferritic stainless steel grades, while six cross-section profiles were considered in duplex stainless steel. The proportions of the sections ranged between the values provided in Table 3, which shows that a wide range of cross-section properties were considered. The selected profiles were classified as Class 1, Class 3 and Class 4 cross-sections according to classification rules provided in EN 1993-1-4 [36], thereby allowing the response of columns having stocky, intermediate and slender cross-sections to be explored. It should also be noted that due to the adoption of $f_{2,\theta}$ in the new cross-section instability assessment rules introduced in Subsection 3.1.1, the considered Class 3 cross-sections according to EN 1993-1-2 [1] fall into the ‘slender’ category, for which the effective cross-section areas A_{eff} were used in the calculations. A summary of all the parameters considered in the calibration is provided in Table 4. Note that, as indicated in the table, the cross-section sizes were selected to cover Class 1, Class 3 and Class 4 profiles, according to the slenderness limits given in EN 1993-1-4 [36]; the web thicknesses of some sections were increased to achieve the target section class. The calibrated values of the imperfection factor α and auxiliary coefficient β for the new design rules are shown in Table 5. In the following subsection, the accuracy of the new proposals is assessed. It should be noted that in this paper, uniformly heated, axially unrestrained pin-ended stainless steel columns with symmetric I-sections were considered as the basic design case, following the approach used in the development of the fire design rules for carbon steel columns [38, 39] in EN 1993-1-2 [1].

5.4. Assessment of the accuracy and reliability of new proposals

In this subsection, the accuracy and reliability of the new design proposals are assessed against the results obtained from nonlinear finite element modelling. The new proposals are also compared against EN 1993-1-2 [1] and the design method recommended by Lopes et al. [2] for the flexural buckling assessment of stainless steel columns at elevated temperatures.

The accuracy of the new proposals is shown in Fig. 15 and Fig. 16 for a series of stainless steel columns experiencing flexural buckling about the major and minor axes, respectively. Note that the room temperature results (i.e. those for 20°C) were included in the figures for reference only. In Fig. 15 and Fig. 16, seven cross-sections were considered for both the austenitic and ferritic stainless steel grades, while six cross-sections were considered for the duplex grade; the cross-section proportions ranged between the values given in Table 3. As can be seen from both figures, the new proposals lead to generally safe-sided and accurate

ultimate strength predictions for stainless steel columns for over the wide considered range of elevated temperature levels, non-dimensional slendernesses, cross-section proportions, axes of buckling and stainless steel grades. The use of ξ_θ in the definition of the generalised imperfection factor η_θ^* results in multiple buckling curves that generally lie lower with increasing temperature. Very accurate results were achieved for non-slender cross-sections, as shown previously in Fig. 10 for an HEM 100 section, while accurate but somewhat more conservative estimations were observed in Fig. 15 and Fig. 16 for cross-sections falling into the ‘slender’ category according to the cross-section classification criteria described in Subsection 3.1.1.

The accuracy of the new proposals is also illustrated in Table 6 for 2200 columns for elevated temperature levels ranging between 200°C and 800°C in increments of 200°C, considering the array of cross-sections previously described with the range of proportions shown in Table 3. In the table, ϵ_{av} , ϵ_{COV} , ϵ_{max} and ϵ_{min} are the average, coefficient of variation, maximum and minimum values of the ratios of the ultimate strength predictions obtained through GMNIA $N_{Ed,max,FE}$ and the proposed design method $N_{Ed,max,prop}$, respectively. Since $\epsilon = N_{Ed,max,FE}/N_{Ed,max,prop}$, ϵ values less than 1.0 indicate strength predictions on the unsafe side. Table 3 shows that the new proposals lead to generally safe-sided ultimate strength predictions for all the considered wide range of stainless steel columns. Additionally, the accuracy of the current rules provided in EN 1993-1-2 and the design proposal made by Lopes et al. [2] is also investigated in Table 6. As can be seen from the table, EN 1993-1-2 [1] leads to very unsafe strength predictions for stainless steel columns in fire. The proposals of Lopes et al. [2], in which the elevated temperature strength at 2% strength $f_{2,\theta}$ was adopted as in the present study, also lead to generally safe-sided strength predictions. However, they are somewhat overly-conservative and also less consistent than the column design rules developed in this study.

In Table 7, the reliability of the new column buckling design proposals is assessed considering the three reliability criteria put forward by Kruppa [40] for the design of steel members in fire. Criterion 1 of [40] states that none of the strength predictions $N_{Ed,max,prop}$ should exceed the FE results $N_{Ed,max,FE}$ by more than 15%, i.e. $(N_{Ed,max,prop} - N_{Ed,max,FE})/N_{Ed,max,FE} \leq 15\%$. Criterion 2 states that less than 20% of the design predictions should be on the unsafe side, i.e. $num(N_{Ed,max,prop} > N_{Ed,max,FE})/num(N_{Ed,max,FE}) \leq 20\%$. Finally, Criterion 3 states that the design predictions should be safe-sided on average, i.e. $\bar{X}[(N_{Ed,max,prop} - N_{Ed,max,FE})/N_{Ed,max,FE}] < 0\%$. In Table 7, the percentage of the columns for which the overpredictions of resistance exceeded 15% of those of GMNIA is shown under the Criterion 1, the percentage of the columns whose ultimate strengths were overpredicted is shown under Criterion 2 and the average percentage of the differences between the design and GMNIA ultimate strengths is shown under Criterion 3. As can be seen from Table 7, the new proposals satisfy all three reliability criteria set out by [40], as does the method of Lopes et al. [2]. On the other hand, EN 1993-1-2 generally fails to fulfill the three reliability criteria for the design of stainless steel columns in fire.

Finally, the accuracy of the new proposal is assessed against that of EN 1993-1-2 [1] and the method of Lopes et al. [2] in Fig. 17 for all the considered 2200 stainless steel columns buckling about the major and minor axis in this study. As can be seen from the figure, the

new proposals lead to significantly enhanced accuracy relative to the existing methods for the flexural buckling assessment of stainless steel columns in fire.

6. Adoption of elevated temperature strength 0.2% proof strength $f_{p0.2,\theta}$ for the design of stainless steel columns in fire

To maintain consistency with the existing design rules in EN 1993-1-2 for carbon steel columns in fire, the new stainless steel column buckling proposals were developed adopting the elevated temperature strength at 2% total strain $f_{2,\theta}$ in Section 5. In this section, alternatively, the use of the elevated temperature 0.2% proof strength $f_{p0.2,\theta}$ is investigated as the basis for the design of stainless steel columns in fire, as utilised for the room temperature design of stainless steel columns in EN 1993-1-4 [36]. The alternative effective width formulations and classification limits developed on the basis of the elevated temperature 0.2% proof strength $f_{p0.2,\theta}$ can be found in Xing et al. [30].

6.1. Column buckling assessment based on elevated temperature 0.2% proof strength $f_{p0.2,\theta}$

Utilising the elevated temperature 0.2% proof strength $f_{p0.2,\theta}$, the following equations can be used for the design of stainless steel columns in fire:

$$\begin{aligned} N_{b,fi,t,Rd} &= \frac{\chi_{fi} A k_{p0.2,\theta} f_y}{\gamma_{M,fi}} \quad \text{for non-slender sections,} \\ N_{b,fi,t,Rd} &= \frac{\chi_{fi} A_{eff} k_{p0.2,\theta} f_y}{\gamma_{M,fi}} \quad \text{for slender sections,} \end{aligned} \quad (37)$$

in which

$$\begin{aligned} \chi_{fi} &= \frac{1}{\phi_\theta + \sqrt{\phi_\theta^2 + \beta \bar{\lambda}_\theta^2}} \quad \text{but} \quad \chi_{fi} \leq 1.0 \\ \text{where} \quad \phi_\theta &= 0.5 \left[1 + \alpha (\bar{\lambda}_\theta - \bar{\lambda}_{\theta,0}) / \xi_\theta + \beta \bar{\lambda}_\theta^2 \right], \end{aligned} \quad (38)$$

in which $\bar{\lambda}_{\theta,0}$ is the plateau slenderness below which $\chi_{fi} = 1.0$, $\xi_\theta = \sqrt{k_{p0.2,\theta}/k_{E,\theta}}$ is the elevated temperature strength-to-stiffness ratio reduction factor and $\bar{\lambda}_\theta$ is the elevated temperature non-dimensional slenderness calculated as

$$\begin{aligned} \bar{\lambda}_\theta &= \bar{\lambda} \xi_\theta = \sqrt{\frac{A f_y}{N_{cr}}} \sqrt{\frac{k_{p0.2,\theta}}{k_{E,\theta}}} \quad \text{for non-slender section,} \\ \bar{\lambda}_\theta &= \bar{\lambda} \xi_\theta = \sqrt{\frac{A_{eff} f_y}{N_{cr}}} \sqrt{\frac{k_{p0.2,\theta}}{k_{E,\theta}}} \quad \text{for slender sections.} \end{aligned} \quad (39)$$

Note that A_{eff} is the effective area determined using the expressions provided in [30]. The calibrated values of α , β and $\bar{\lambda}_{\theta,0}$ are provided in Table 8.

For stocky columns with $\bar{\lambda}_\theta \leq 0.1$ and non-slender sections, both local and global instability effects were found to be insignificant in this study. Thus, the ultimate cross-section strength $N_{fi,\theta,Rd}$ of such members can be determined on the basis of elevated temperature strength at 2% total strain $f_{2,\theta}$ as given below:

$$N_{fi,\theta,Rd} = \frac{Ak_{2,\theta}f_y}{\gamma_{M,fi}} \quad \text{for members with } \bar{\lambda}_\theta \leq 0.1 \text{ and non-slender sections.} \quad (40)$$

Note though that $N_{fi,\theta,Rd}$ can also be conservatively taken as $N_{fi,\theta,Rd} = Ak_{p0.2,\theta}f_y/\gamma_{M,fi}$ for short columns with $\bar{\lambda}_\theta \leq 0.1$.

The ultimate strength predictions determined through the described alternative method adopting $f_{p0.2,\theta}$ are compared against those of GMNIA for a wide range of stainless steel columns in fire in Fig. 18 and Fig. 19 for major axis and minor axis buckling respectively, considering the full set of results described earlier across the range of proportions summarised in Table 3. As can be seen from the figures, the alternative method leads to safe ultimate strength estimations with a high level of accuracy. The use of the ultimate cross-section strength based on the elevated temperature strength at 2% total strain $f_{2,\theta}$ for members with $\bar{\lambda}_\theta \leq 0.1$ and non-slender sections results in accurate strength predictions for stocky members as shown in Fig. 18 and Fig. 19.

Based on the observations made in this section, it can be stated that the adoption of the elevated temperature 0.2% proof strength $f_{p0.2,\theta}$ leads to high accuracy for the design of stainless steel columns in fire. However, this approach is both (i) inconsistent with the existing design rules for the buckling assessment of carbon steel columns in fire given in EN 1993-1-2 [1] and (ii) requires the use of the elevated temperature strength at 2% for stocky columns with Class 1, 2 and 3 sections to avoid large underpredictions of ultimate strength, thus leading to a design procedure with two different reference strengths (i.e. $f_{0.2p,\theta}$ and $f_{2,\theta}$), which is less desirable from a practical viewpoint. Therefore, for the purpose of developing safe, practical and accurate design rules for stainless steel columns in fire that are consistent with the existing rules given in EN 1993-1-2 [1] for carbon steel columns, the elevated temperature strength $f_{2,\theta}$ at 2% total strain remains the recommended basis for the design rules, as set out in Section 5.

7. Conclusions

In this paper, new proposals for the design of stainless steel I-section columns in fire, compatible with the existing design methods for carbon steel columns given in EN 1993-1-2 [1] have been developed. Shell finite element models of stainless steel welded I-section columns able to replicate their behaviour at elevated temperatures were created and validated against existing experimental results from the literature; further experimental data is considered necessary in this area. Using the validated finite element models, the accuracy of the rules given in EN 1993-1-2 [1] for the flexural buckling assessment of stainless steel columns in fire was examined. It was shown that the current EN 1993-1-2 rules [1] lead to significant overpredictions of member resistance, which was ascribed to the dependency of the generalised imperfection factor used in these equations on the temperature level. A new

expression for the generalised imperfection factor independent of the temperature level in accordance with the Perry-Robertson concept [34, 35] adopted in EN 1993-1-2 [1] was put forward. Using the new expression for the generalised imperfection factor and adopting the elevated temperature strength at 2% total strain $f_{2,\theta}$ as the basic design strength to maintain the consistency with the carbon steel column design rules in EN 1993-1-2 [1], new flexural buckling assessment rules for stainless steel columns in fire were calibrated considering a range of elevated temperature levels, cross-section geometries, slendernesses and stainless steel grades. The reliability of the new proposals was assessed against the fire design reliability criteria set out by Kruppa [40], which were shown to be satisfied. The new proposals made herein are due to be incorporated into the upcoming version of EN 1993-1-2.

References

- [1] EN 1993-1-2, Eurocode 3 Design of steel structures-Part 1-2: General rules – Structural fire design. European Committee for Standardization (CEN), Brussels; 2005.
- [2] Lopes, N., Real, P., da Silva, L., Franssen, J.M.. Axially loaded stainless steel columns in case of fire. *Journal of Structural Fire Engineering* 2010;1(1):43–60.
- [3] Yuan, H., Wang, Y., Shi, Y., Gardner, L.. Residual stress distributions in welded stainless steel sections. *Thin-Walled Structures* 2014;79:38–51.
- [4] Gardner, L., Baddoo, N.. Fire testing and design of stainless steel structures. *Journal of Constructional Steel Research* 2006;62(6):532–543.
- [5] Ng, K., Gardner, L.. Buckling of stainless steel columns and beams in fire. *Engineering Structures* 2007;29(5):717–730.
- [6] Gardner, L.. Stainless steel structures in fire. *Proceedings of the Institution of Civil Engineers - Structures and Buildings* 2007;160(3):129–138.
- [7] Uppfeldt, B., Ala-Outinen, T., Veljkovic, M.. A design model for stainless steel box columns in fire. *Journal of Constructional Steel Research* 2008;64(11):1294–1301.
- [8] Tondini, N., Rossi, B., Franssen, J.M.. Experimental investigation on ferritic stainless steel columns in fire. *Fire Safety Journal* 2013;62:238–248.
- [9] Liu, M., Fan, S., Ding, R., Chen, G., Du, E., Wang, K.. Experimental investigation on the fire resistance of restrained stainless steel h-section columns. *Journal of Constructional Steel Research* 2019;163:105770.
- [10] Ding, R., Fan, S., Chen, G., Li, C., Du, E., Liu, C.. Fire resistance design method for restrained stainless steel h-section columns under axial compression. *Fire Safety Journal* 2019;102837.
- [11] Fan, S., Liu, M., Sun, W., Guo, Y., Han, Y.L.. Experimental investigation of eccentrically compressed stainless steel columns with constraints in fire. *Fire Safety Journal* 2018;99:49–62.
- [12] Lopes, N., Manuel, M., Sousa, A.R., Real, P.V.. Parametric study on austenitic stainless steel beam-columns with hollow sections under fire. *Journal of Constructional Steel Research* 2019;152:274–283.
- [13] Mohammed, A., Afshan, S.. Numerical modelling and fire design of stainless steel hollow section columns. *Thin-Walled Structures* 2019;144:106243.
- [14] Abaqus v.6.14 Reference Manual. Simulia, Dassault Systemes; 2014.
- [15] EN 1993-1-5, Eurocode 3 Design of steel structures-Part 1-5: Plated structural elements. European Committee for Standardization (CEN), Brussels; 2005.
- [16] Structural Stainless Steel Design Manual, Fourth Edition. Steel Construction Institute (SCI); 2017.
- [17] Gardner, L., Insausti, A., Ng, K., Ashraf, M.. Elevated temperature material properties of stainless steel alloys. *Journal of Constructional Steel Research* 2010;66(5):634–647.
- [18] Gardner, L., Bu, Y., Francis, P., Baddoo, N., Cashell, K., McCann, F.. Elevated temperature material properties of stainless steel reinforcing bar. *Construction and Building Materials* 2016;114:977–997.

- [19] European Commission. Stainless steel in fire. Final report. Directorate-General for Research and Innovation, EUR 23745; 2009.
- [20] Ala-Outinen, T., Oksanen, T.. Stainless steel compression members exposed to fire. Research Notes 1864, Technical Research Centre of Finland (VTT), Finland; 1997.
- [21] Ramberg, W., Osgood, W.R.. Description of stress-strain curves by three parameters. Technical note no. 902, National Advisory Committee on Aeronautics (NACA); 1943.
- [22] Afshan, S., Zhao, O., Gardner, L.. Standardised material properties for numerical parametric studies of stainless steel structures and buckling curves for tubular columns. *Journal of Constructional Steel Research* 2019;152:2–11.
- [23] Liang, Y., Manninen, T., Zhao, O., Walport, F., Gardner, L.. Elevated temperature material properties of a new high-chromium austenitic stainless steel. *Journal of Constructional Steel Research* 2019;152:261–273.
- [24] Jandera, M., Gardner, L., Machacek, J.. Residual stresses in cold-rolled stainless steel hollow sections. *Journal of Constructional Steel Research* 2008;64(11):1255–1263.
- [25] Crisfield, M.A.. A fast incremental/iterative solution procedure that handles “snap-through”. *Computers & Structures* 1981;13(1-3):55–62.
- [26] Ramm, E.. Strategies for tracing the nonlinear response near limit points. In: *Nonlinear finite element analysis in structural mechanics*. Springer; 1981, p. 63–89.
- [27] Pauli, J., Somaini, D., Knobloch, M., Fontana, M.. Experiments on steel columns under fire conditions. IBK test report no. 340; Institute of Structural Engineering (IBK), ETH Zurich; 2012.
- [28] Kucukler, M., Gardner, L., Bu, Y.. Flexural torsional buckling of austenitic stainless steel i-section beam-columns: Testing, numerical modelling and design. *Thin-Walled Structures* 2019;Submitted for publication.
- [29] Bu, Y., Gardner, L.. Finite element modelling and design of welded stainless steel i-section columns. *Journal of Constructional Steel Research* 2019;152:57–67.
- [30] Xing, Z., Kucukler, M., Gardner, L.. Local buckling of stainless steel plates in fire. *Thin-Walled Structures* 2019;Submitted for publication.
- [31] Couto, C., Real, P.V., Lopes, N., Zhao, B.. Effective width method to account for the local buckling of steel thin plates at elevated temperatures. *Thin-Walled Structures* 2014;84:134–149.
- [32] Couto, C., Real, P.V., Lopes, N., Zhao, B.. Resistance of steel cross-sections with local buckling at elevated temperatures. *Journal of Constructional Steel Research* 2015;109:101–114.
- [33] EN 1993-1-1, Eurocode 3 Design of steel structures-Part 1-1: General rules and rules for buildings. European Committee for Standardization (CEN), Brussels; 2005.
- [34] Ayrton, W., Perry, J.. On struts. *The Engineer* 1886;62:464–465.
- [35] Robertson, A.. The strength of struts. *The Institution of Civil Engineers (ICE) – Selected Engineering Papers* 1925;1(28):1–55.
- [36] EN 1993-1-4, Eurocode 3 Design of steel structures-Part 1-2: General rules – Supplementary rules for stainless steel. European Committee for Standardization (CEN), Brussels; 2005.
- [37] Couto, C., Real, P.V., Lopes, N., Zhao, B.. Numerical investigation of the lateral-torsional buckling of beams with slender cross sections for the case of fire. *Engineering Structures* 2016;106:410–421.
- [38] Franssen, J.M., Talamona, D., Kruppa, J., Cajot, L.. Stability of steel columns in case of fire: experimental evaluation. *Journal of Structural Engineering, ASCE* 1998;124(2):158–163.
- [39] Talamona, D., Franssen, J.M., Schleich, J.B., Kruppa, J.. Stability of steel columns in case of fire: Numerical modeling. *Journal of Structural Engineering, ASCE* 1997;123(6):713–720.
- [40] Kruppa, J.. Eurocodes–Fire parts: Proposal for a methodology to check the accuracy of assessment methods. CEN TC 250, Horizontal Group Fire, Document no: 99/130; 1999.

Figures captions

Figure 1 : Local and global imperfections applied to the shell finite element models

Figure 2 : Stress-strain response of different stainless steel grades and carbon steel at elevated temperatures

Figure 3 : Comparison of Young's modulus $k_{E,\theta}$ and strength reduction factors $k_{2,\theta}$, $k_{p0.2,\theta}$ for the different considered stainless steel grades and carbon steel at elevated temperatures

Figure 4 : Residual stress patterns applied to FE models

Figure 5 : Finite element model of a typical stainless steel column

Figure 6 : Comparison between test and FE temperature versus deformation paths for an RHS $150 \times 100 \times 6$ austenitic stainless steel column in fire reported in [4]

Figure 7 : Comparison between furnace temperature versus axial deformation paths determined from the experiments of [8] and the finite elements developed herein for ferritic stainless steel columns in fire

Figure 8 : Comparison between the load versus end-shortening paths obtained from experiments [27] and finite element models for carbon steel I-section columns undergoing flexural buckling in fire

Figure 9 : Comparison between test and FE deformation versus temperature paths for restrained austenitic stainless steel columns in fire reported in [9]

Figure 10 : Accuracy of strength predictions from EN 1993-1-2 and the new design proposal relative to FE results for the flexural buckling of stainless steel columns in fire

Figure 11 : Imperfect pin-ended column used in the derivation of column buckling equations in EN 1993-1-2 [1] following the Perry-Robertson concept

Figure 12 : Equivalent imperfections \bar{e}_0 relative to column lengths L (i.e. \bar{e}_0/L) for austenitic stainless steel and carbon steel columns at different temperatures as adopted in EN 1993-1-2

Figure 13 : Variation of the square root of the elevated temperature strength-to-stiffness ratio factor ξ_θ with temperature for different steel types

Figure 14 : Calibration of generalised imperfection factors $\eta_{\theta*}$ for austenitic stainless steel columns buckling about the major axis in fire

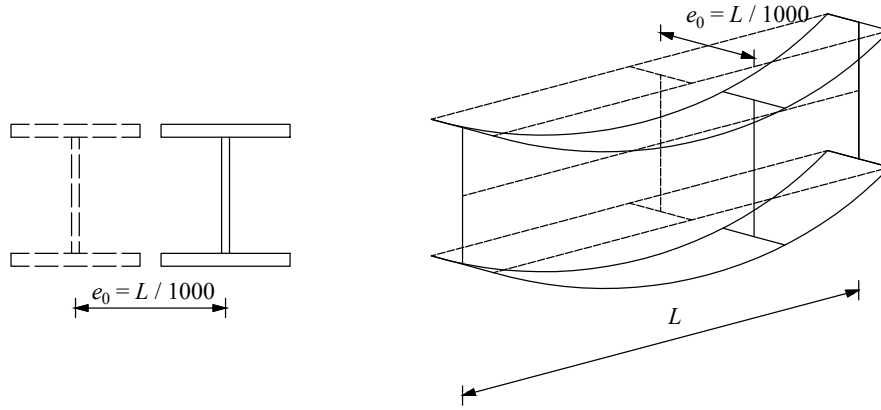
Figure 15 : Accuracy of the new design proposals, based on the elevated temperature strength at 2% total strain, for the major axis flexural buckling assessment of stainless steel columns in fire

Figure 16 : Accuracy of the new design proposals, based on the elevated temperature strength at 2% total strain, for the minor axis flexural buckling assessment of stainless steel columns in fire

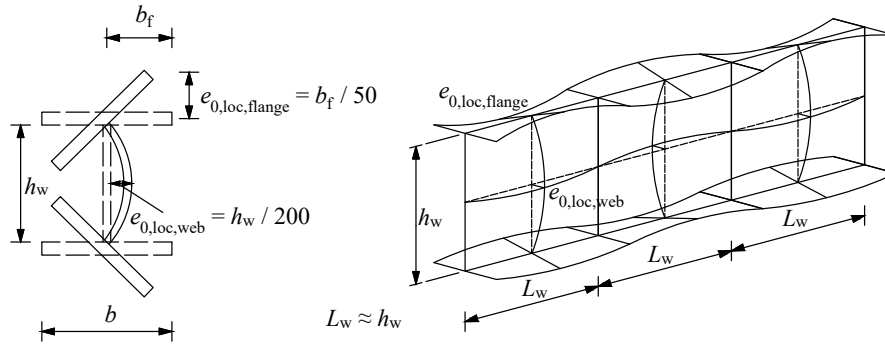
Figure 17 : Comparison of the accuracy of the new proposal against EN 1993-1-2 [1] and the method of Lopes et al. [2] for all stainless steel columns considered in this study

Figure 18 : Accuracy of the alternative design method based on the elevated temperature 0.2% proof strength for the major axis flexural buckling assessment of stainless steel columns in fire

Figure 19 : Accuracy of the alternative design method based on the elevated temperature 0.2% proof strength for the minor axis flexural buckling assessment of stainless steel columns in fire



(a) Global imperfection



(b) Local imperfection

Figure 1: Local and global imperfections applied to the shell finite element models

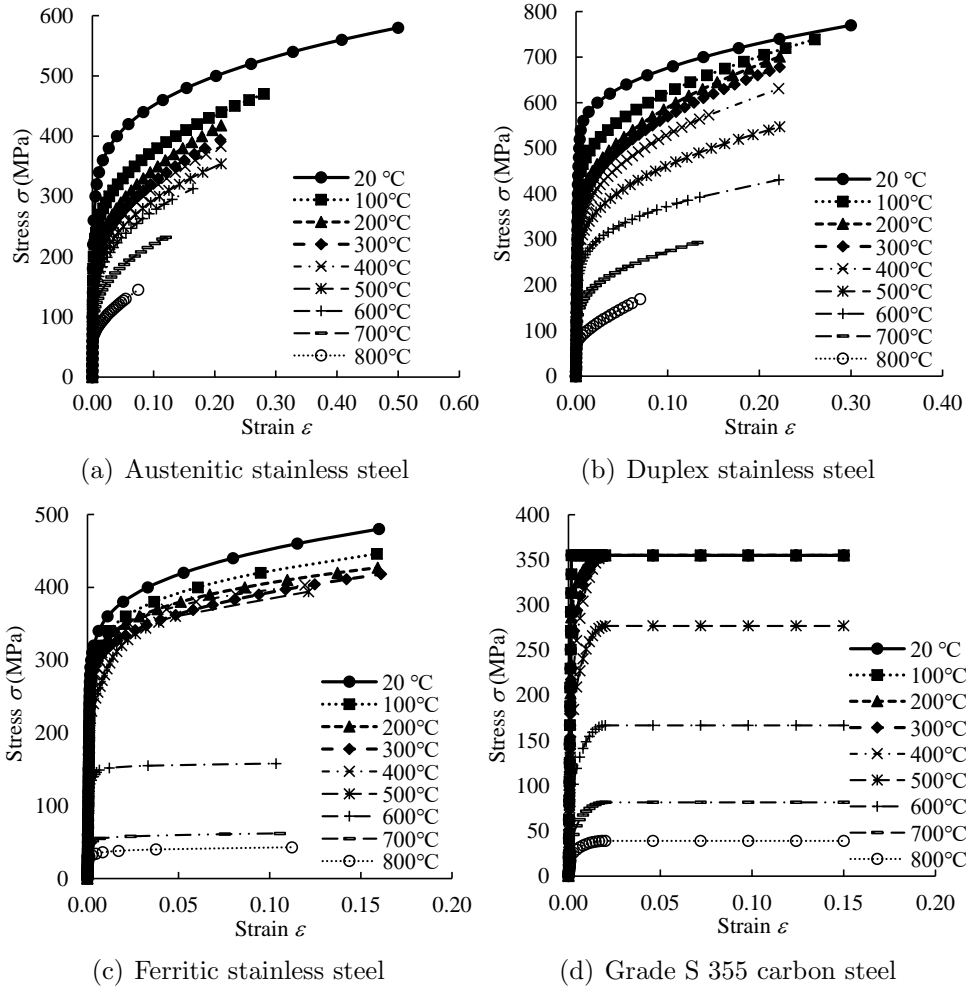


Figure 2: Stress-strain response of different stainless steel grades and carbon steel at elevated temperatures

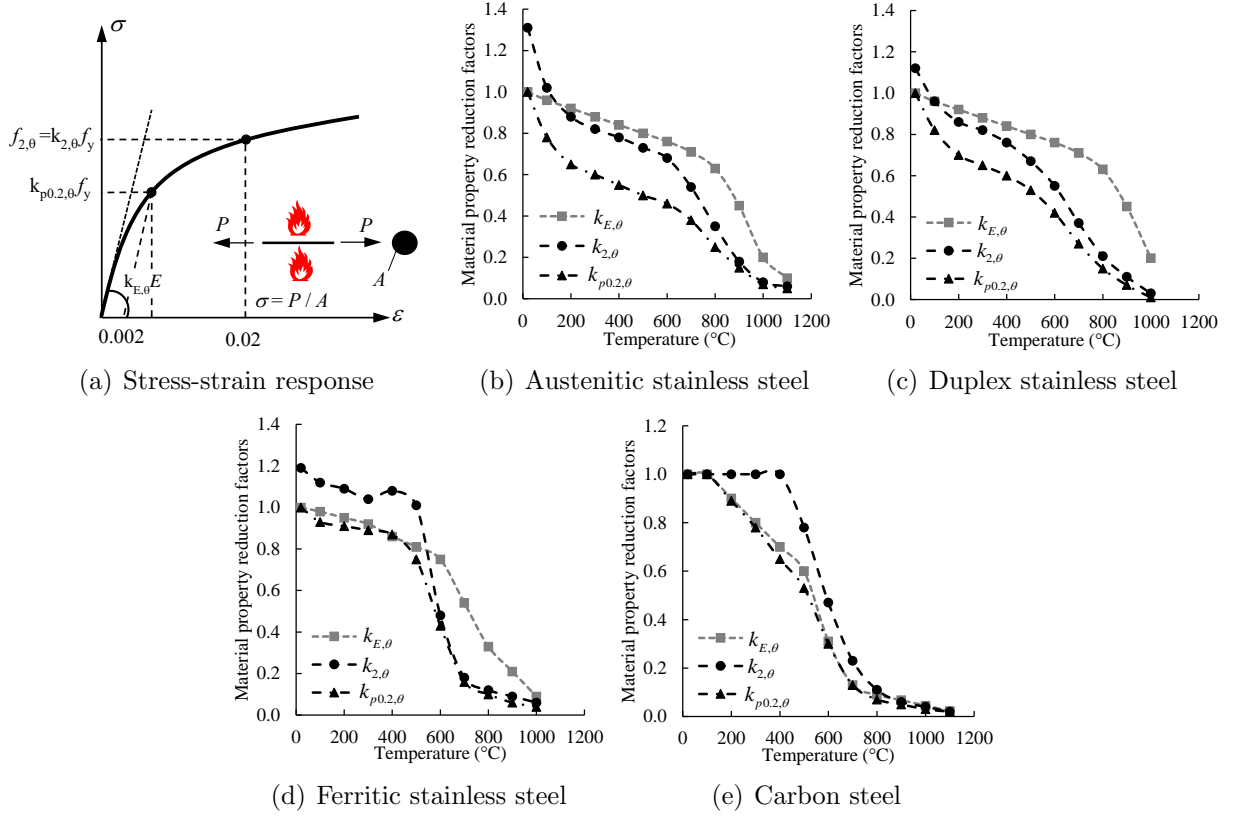


Figure 3: Comparison of Young's modulus $k_{E,\theta}$ and strength reduction factors $k_{2,\theta}$, $k_{p0.2,\theta}$ for the different considered stainless steel grades and carbon steel at elevated temperatures

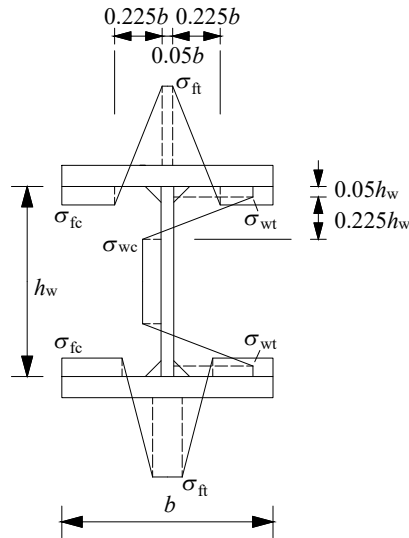


Figure 4: Residual stress patterns applied to FE models

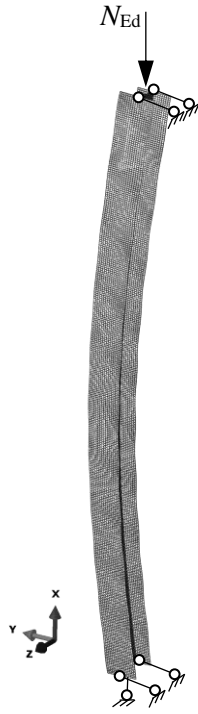


Figure 5: Finite element model of a typical stainless steel column

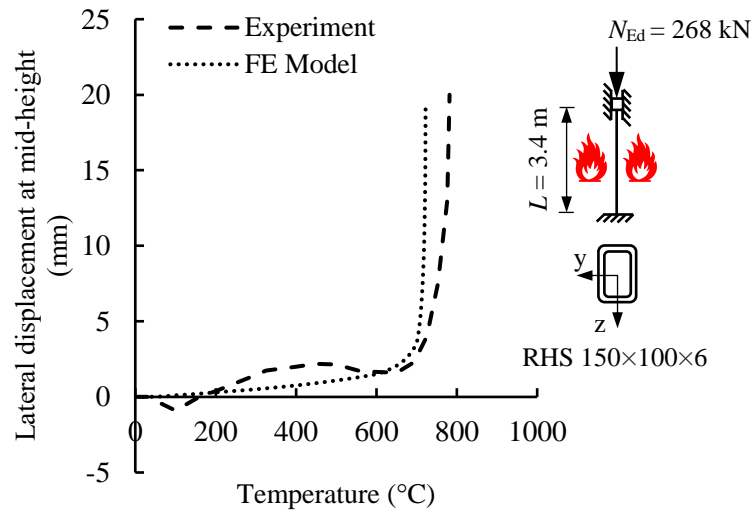


Figure 6: Comparison between test and FE deformation versus temperature paths for an RHS 150×100×6 austenitic stainless steel column in fire reported in [4]

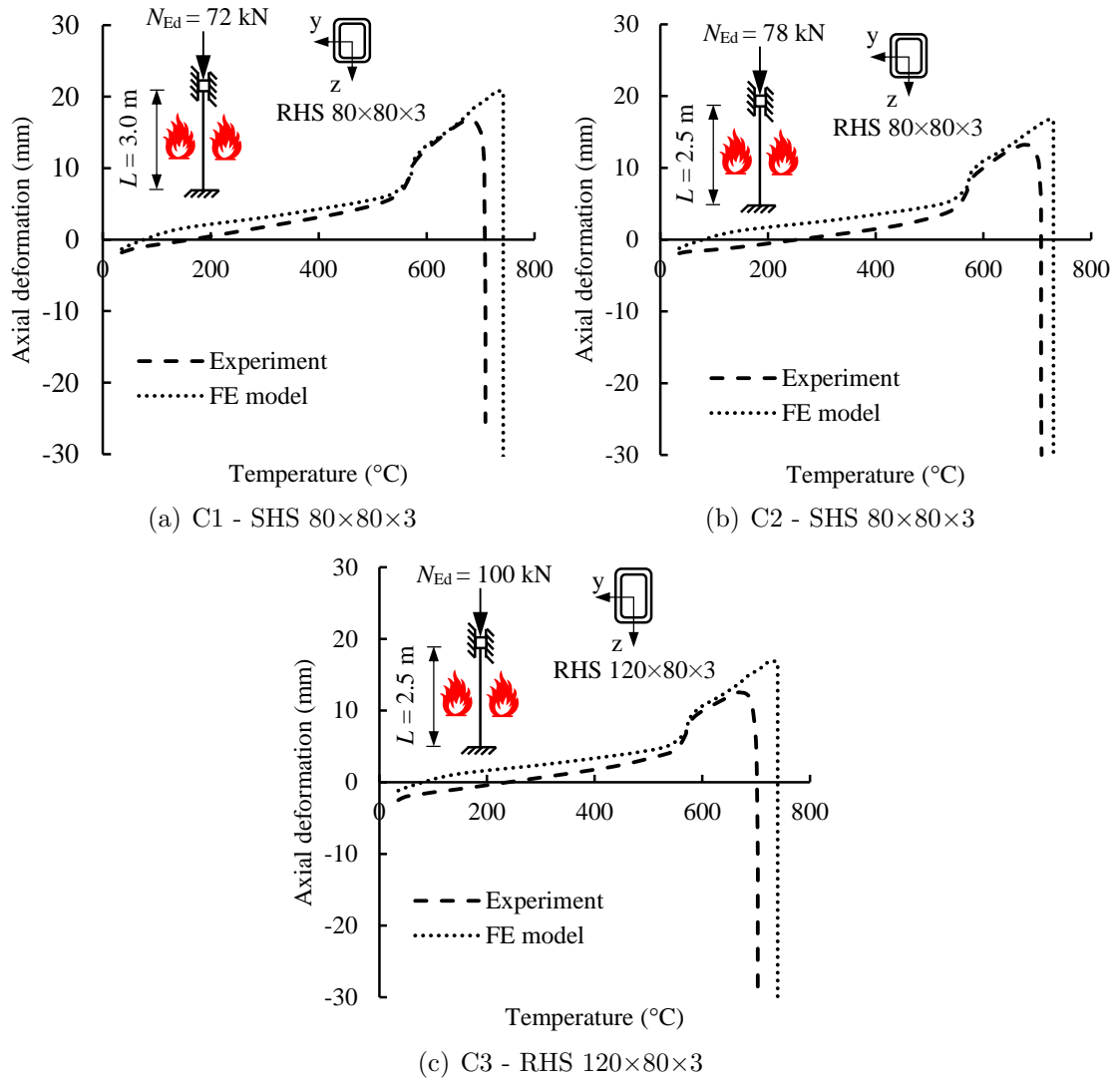


Figure 7: Comparison between furnace temperature versus axial deformation paths determined from the experiments of [8] and the finite elements developed herein for ferritic stainless steel columns in fire

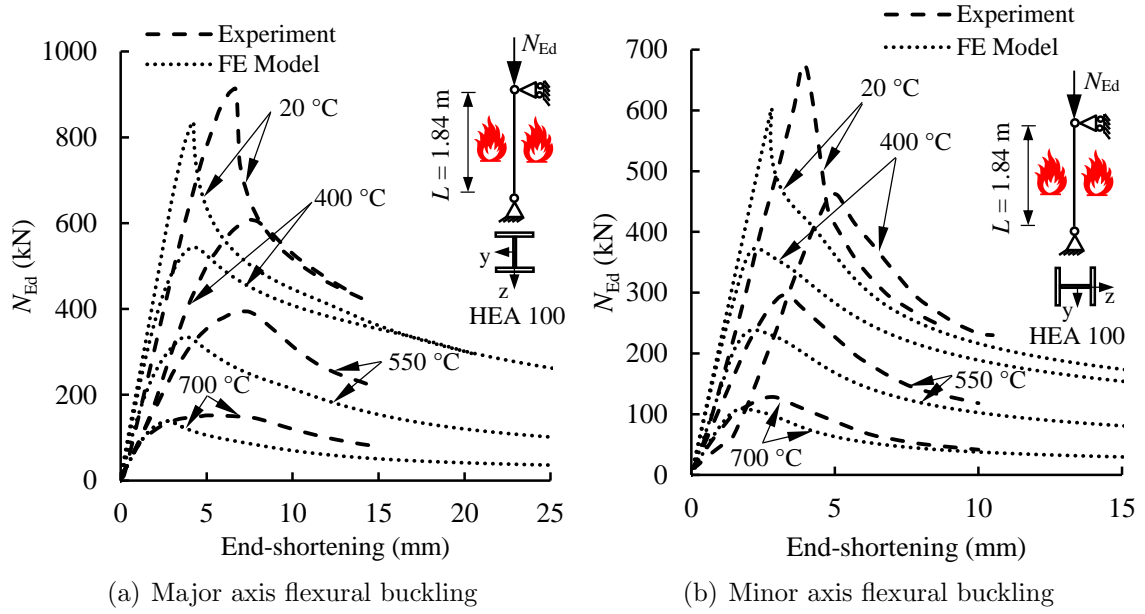
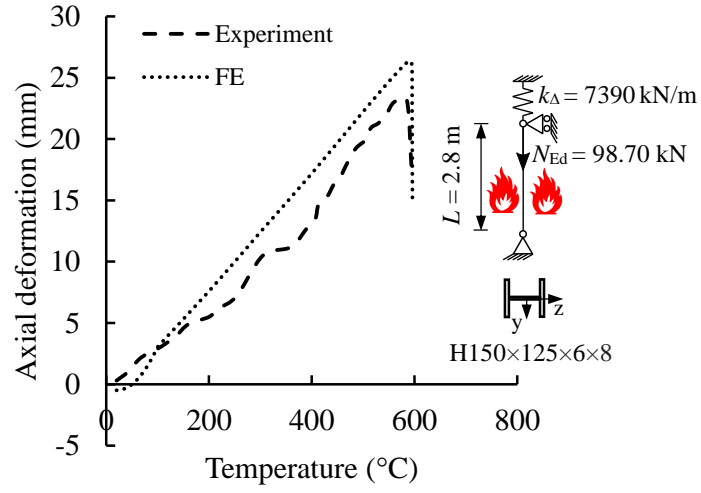
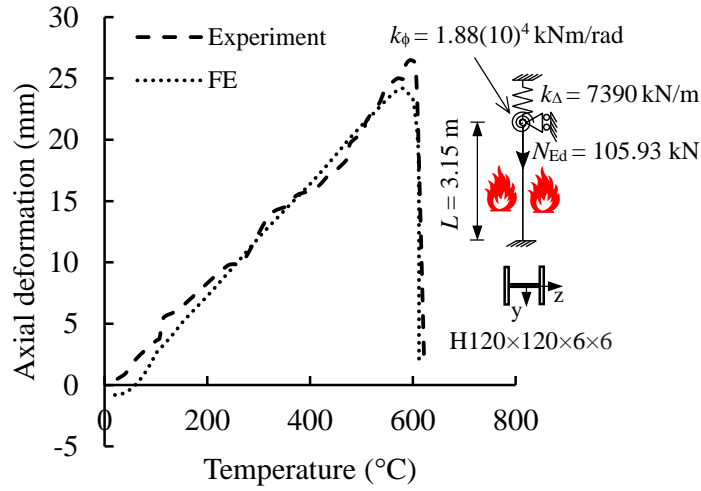


Figure 8: Comparison between the load versus end-shortening paths obtained from experiments [27] and finite element models for carbon steel I-section columns undergoing flexural buckling in fire

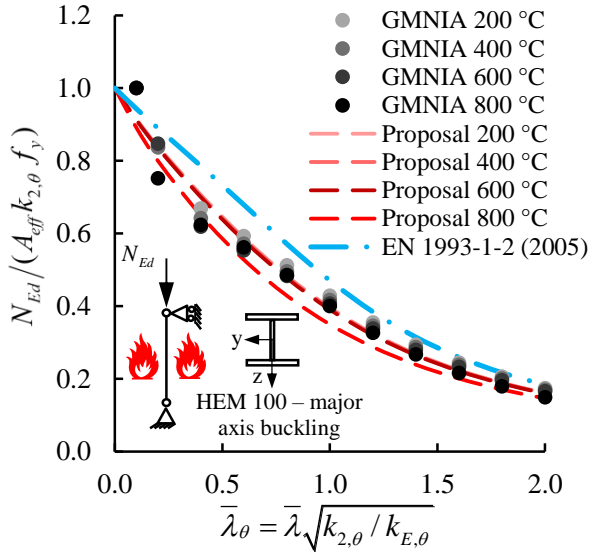


(a) Z4 - H150×125×6×8

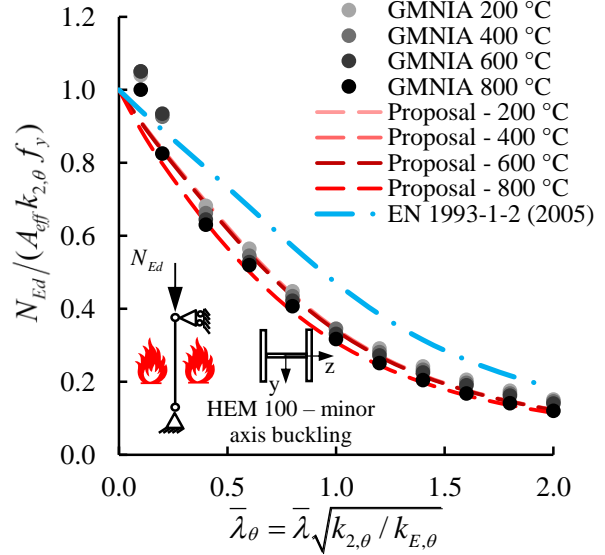


(b) Z7 - H120×120×6×6

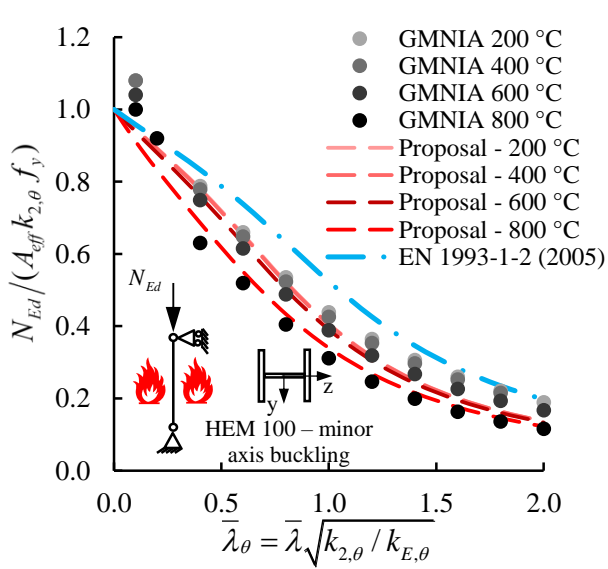
Figure 9: Comparison between test and FE deformation versus temperature paths for restrained austenitic stainless steel columns in fire reported in [9]



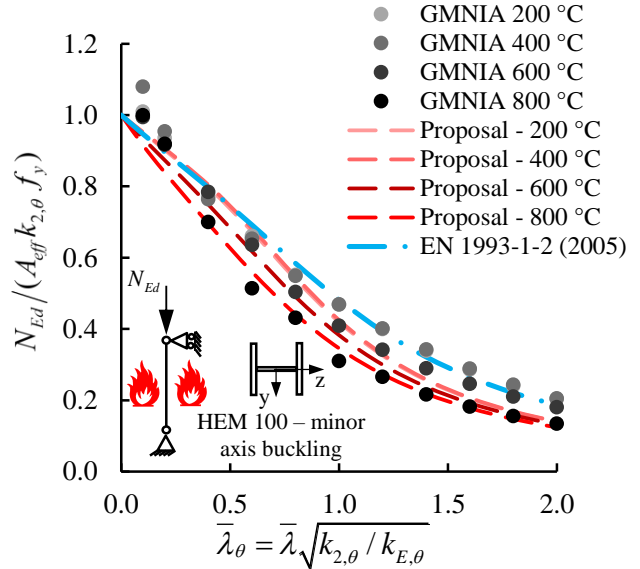
(a) Austenitic stainless steel – major axis buckling



(b) Austenitic stainless steel – minor axis buckling



(c) Duplex stainless steel – minor axis buckling



(d) Ferritic stainless steel – minor axis buckling

Figure 10: Accuracy of strength predictions from EN 1993-1-2 and the new design proposal relative to FE results for the flexural buckling of stainless steel columns in fire

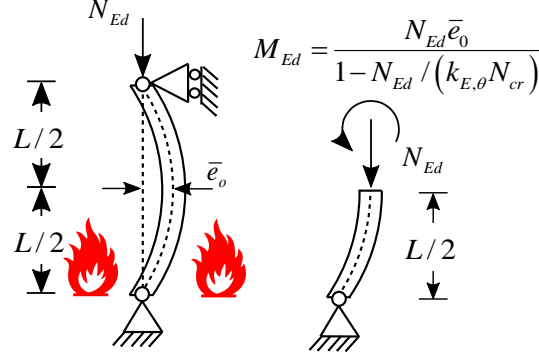


Figure 11: Imperfect pin-ended column used in the derivation of column buckling equations in EN 1993-1-2 [1] following the Perry-Robertson concept

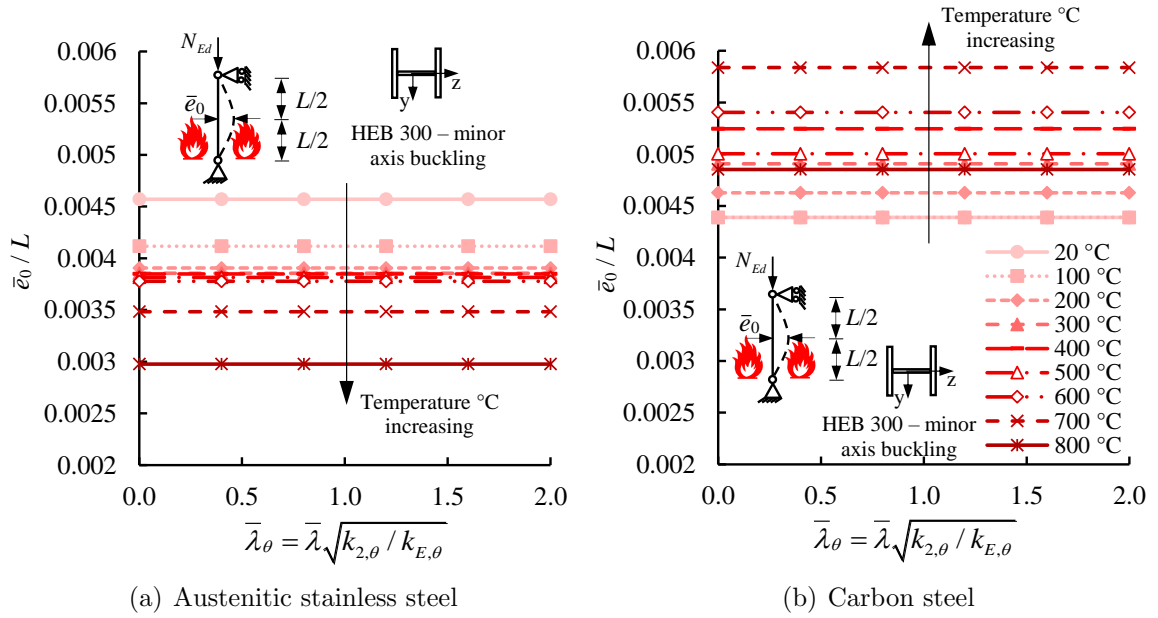


Figure 12: Equivalent imperfections \bar{e}_0 relative to column lengths L (i.e. \bar{e}_0/L) for austenitic stainless steel and carbon steel columns at different temperatures as adopted in EN 1993-1-2

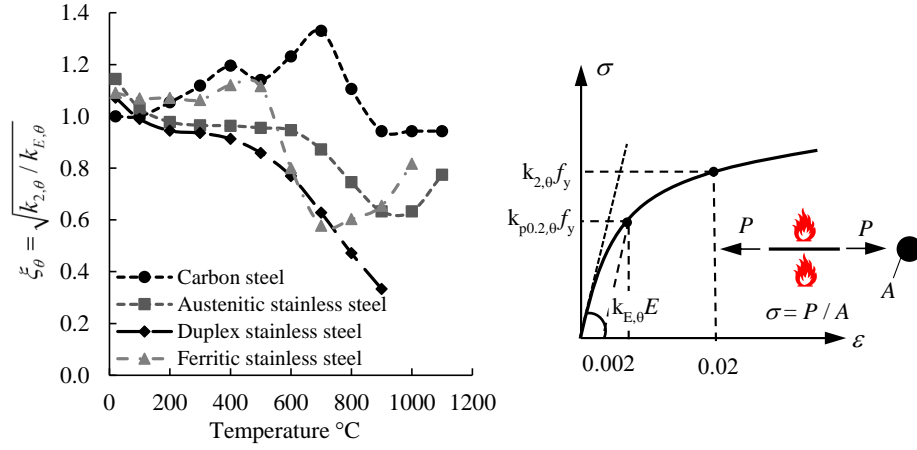


Figure 13: Variation of the square root of the elevated temperature strength-to-stiffness ratio factor ξ_θ with temperature for different steel types

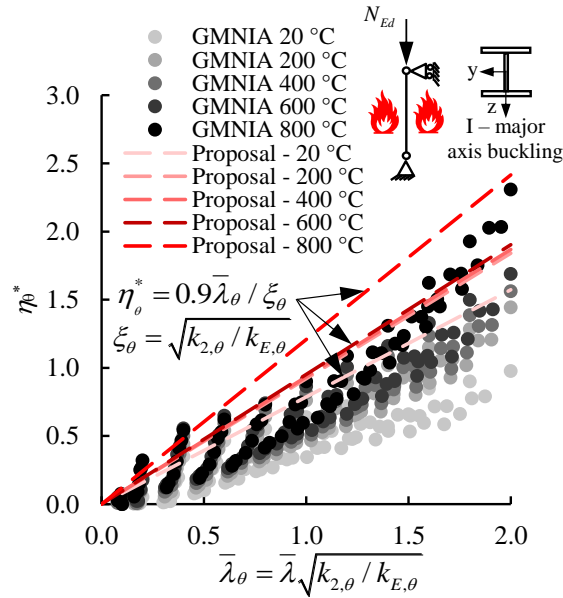


Figure 14: Calibration of generalised imperfection factors η_θ^* for austenitic stainless steel columns buckling about the major axis in fire

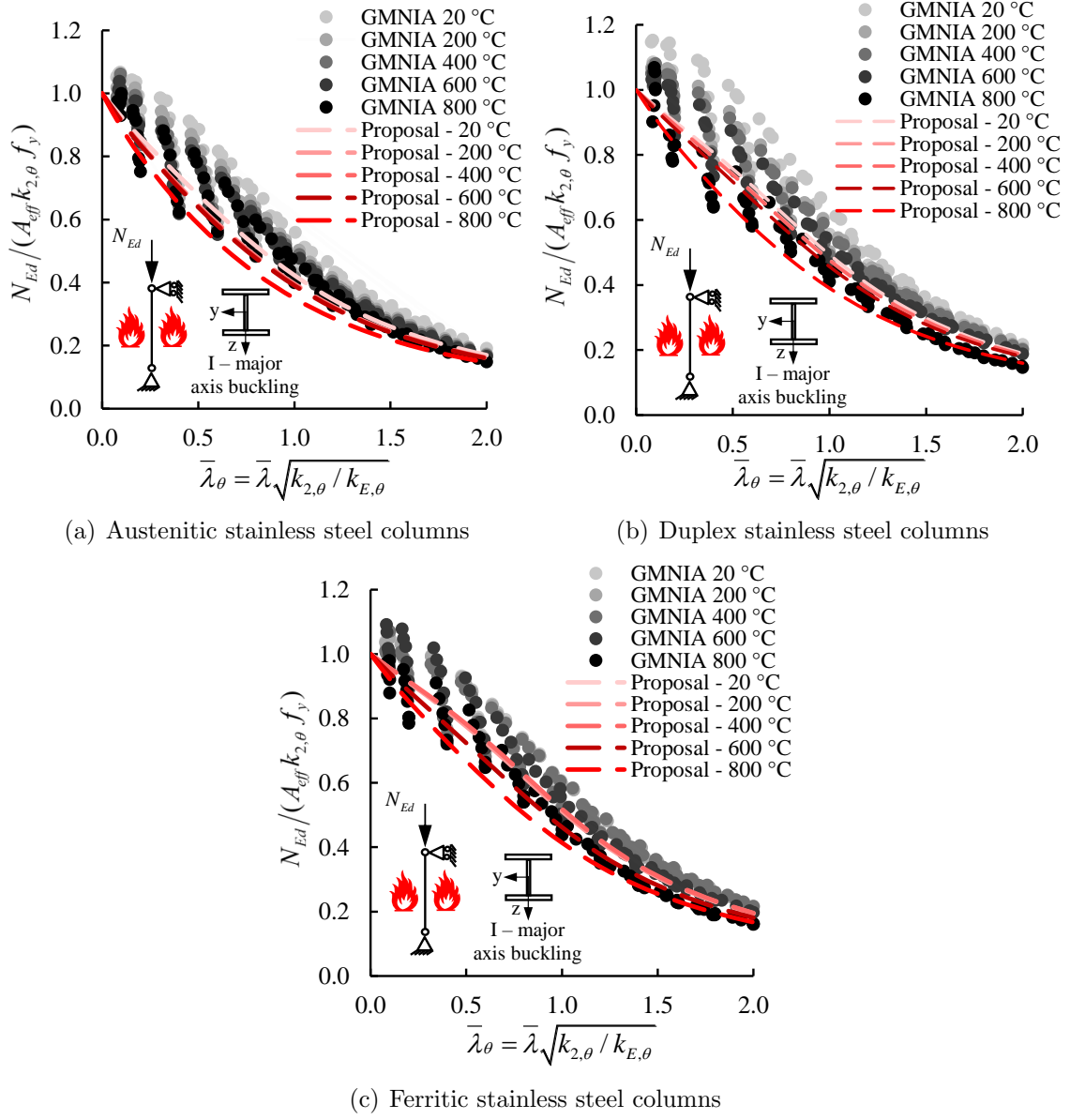
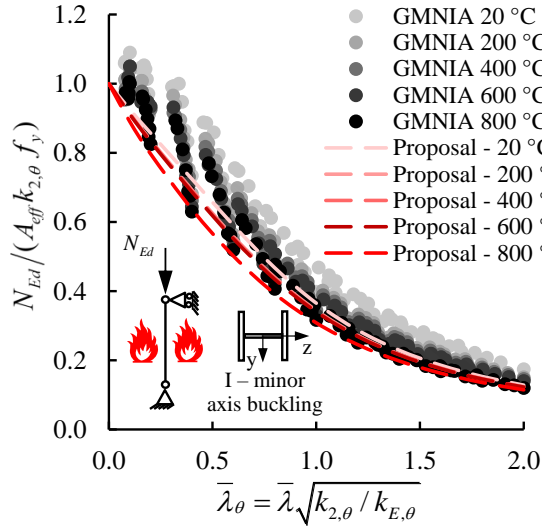
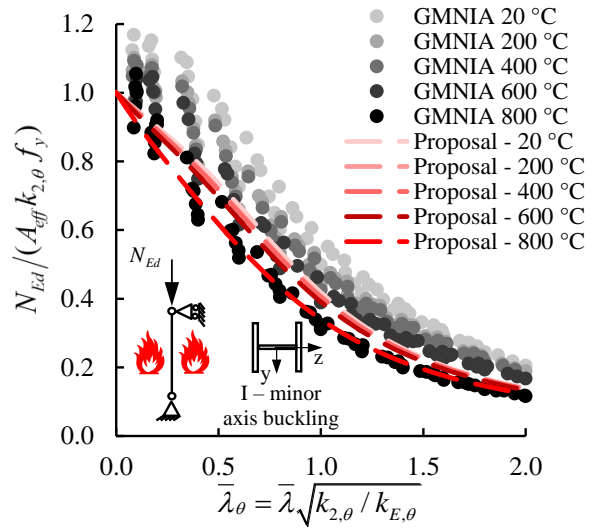


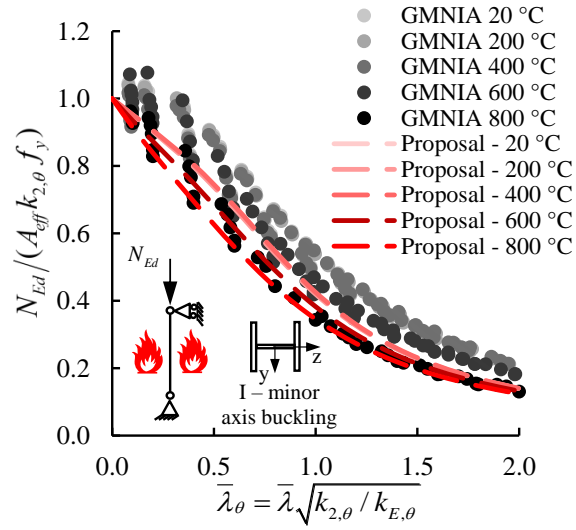
Figure 15: Accuracy of the new design proposals, based on the elevated temperature strength at 2% total strain, for the major axis flexural buckling assessment of stainless steel columns in fire



(a) Austenitic stainless steel columns



(b) Duplex stainless steel columns



(c) Ferritic stainless steel columns

Figure 16: Accuracy of the new design proposals, based on the elevated temperature strength at 2% total strain, for the minor axis flexural buckling assessment of stainless steel columns in fire

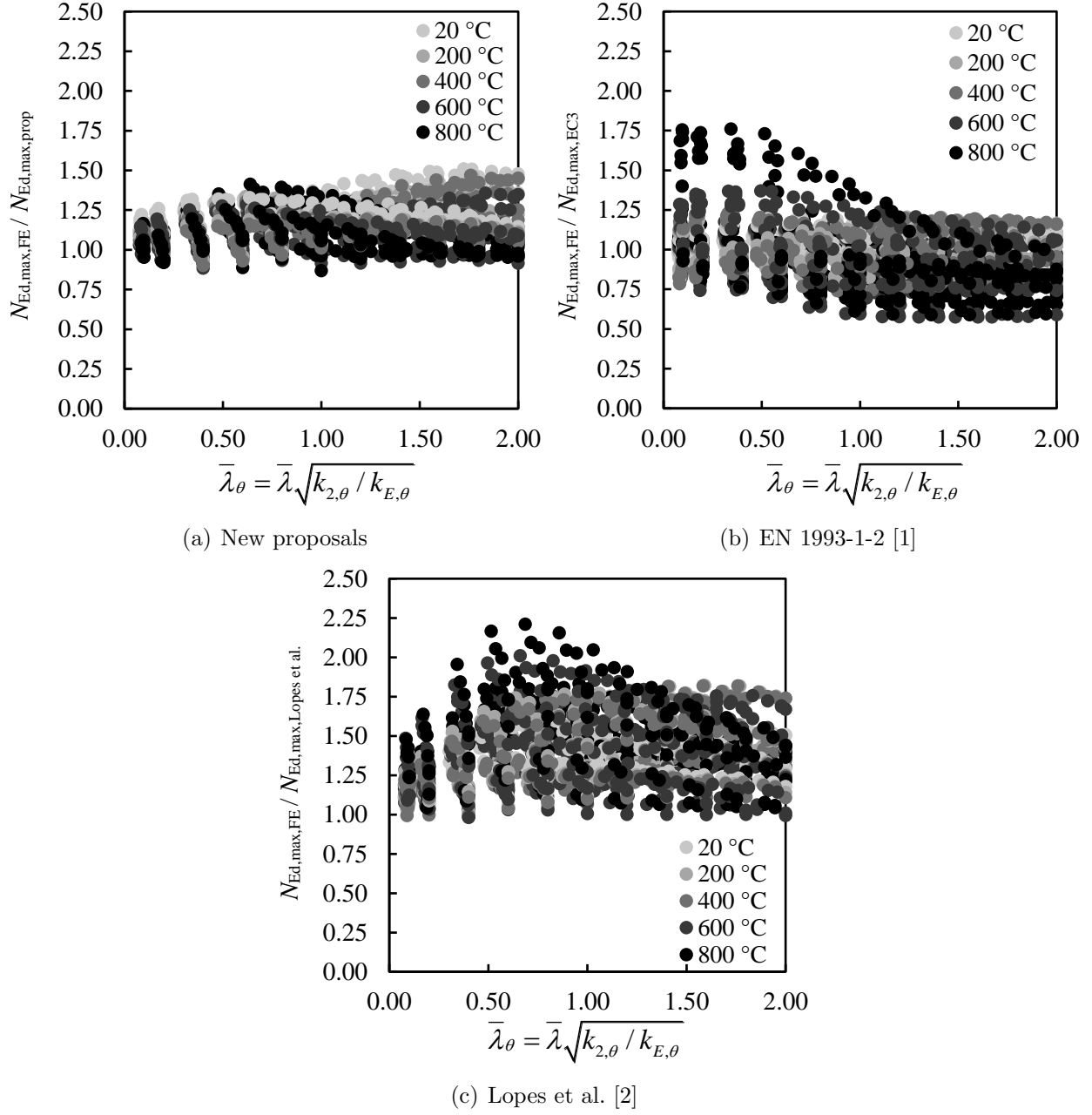
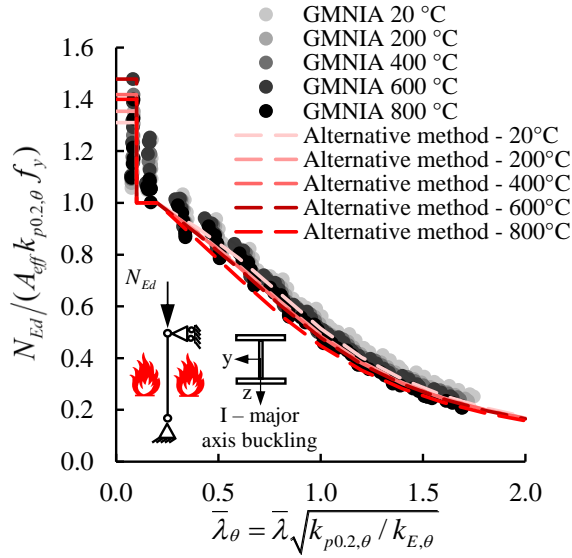
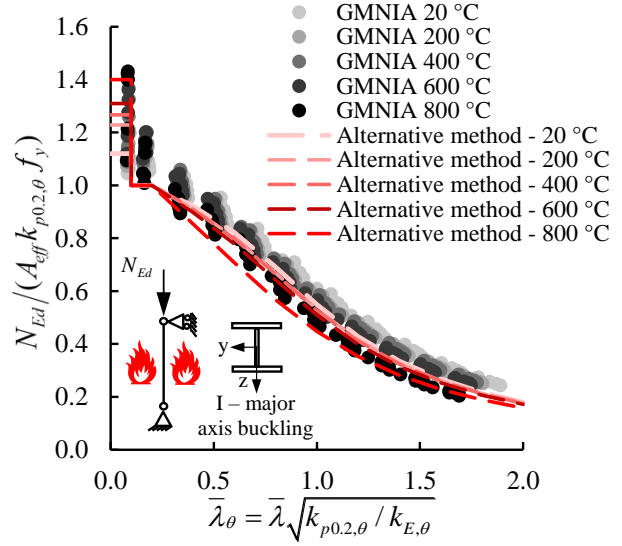


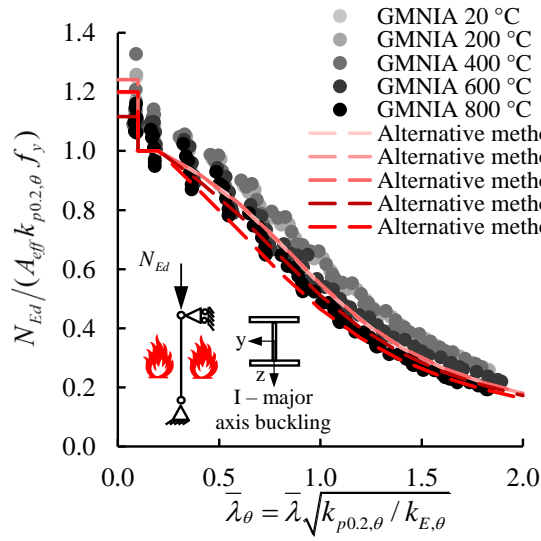
Figure 17: Comparison of the accuracy of the new proposal against EN 1993-1-2 [1] and the method of Lopes et al. [2] for all stainless steel columns considered in this study



(a) Austenitic stainless steel columns

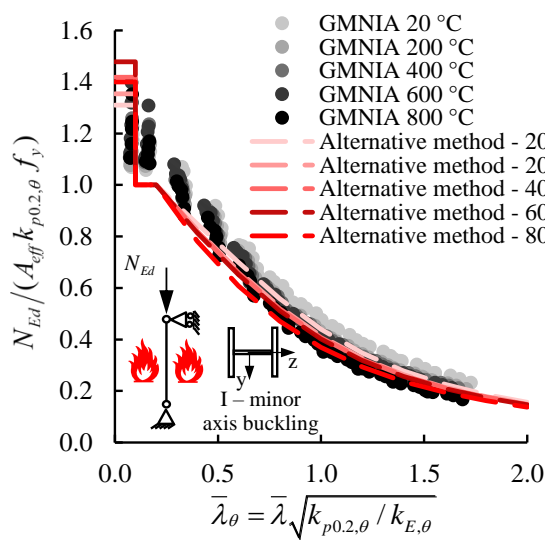


(b) Duplex stainless steel columns

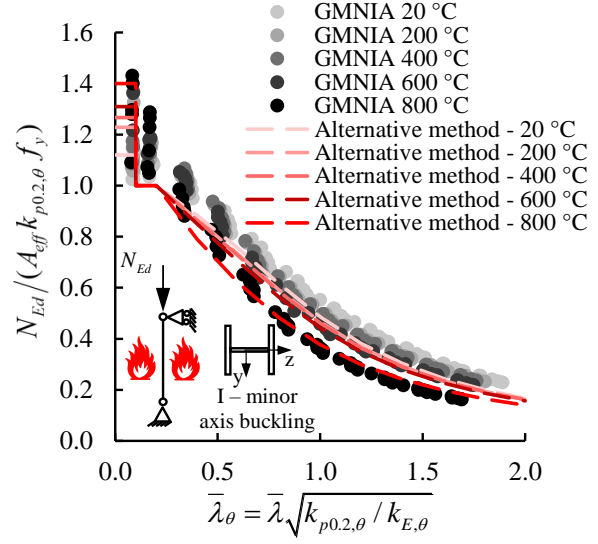


(c) Ferritic stainless steel columns

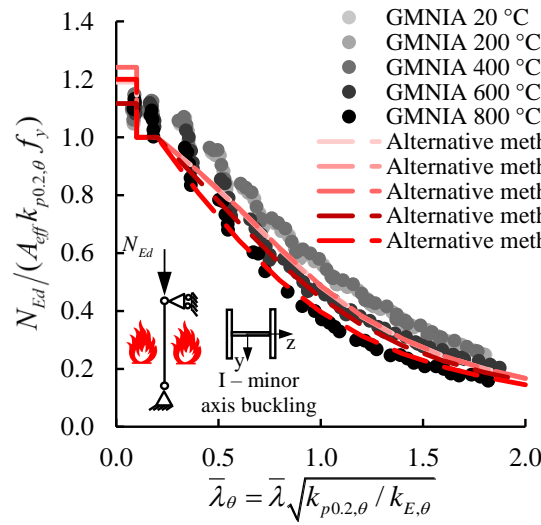
Figure 18: Accuracy of the alternative design method based on the elevated temperature 0.2% proof strength for the major axis flexural buckling assessment of stainless steel columns in fire



(a) Austenitic stainless steel columns



(b) Duplex stainless steel columns



(c) Ferritic stainless steel columns

Figure 19: Accuracy of the alternative design method based on the elevated temperature 0.2% proof strength for the minor axis flexural buckling assessment of stainless steel columns in fire

Tables captions

Table 1 : Comparison between critical temperature values θ_{cr} obtained through experiments [4, 8, 20] and finite element models for stainless steel columns in fire

Table 2 : Comparison of load carrying capacities of simply-supported HEA 100 carbon steel columns in fire determined by Pauli et al. [27] $N_{u,test}$ and finite element models created in this paper $N_{u,FE}$

Table 3 : Range of the proportions of the cross-sections considered in the calibration

Table 4 : Summary of the parameters considered in the numerical studies used for the development and assessment of design method put forward in this paper

Table 5 : Calibrated values of imperfection factor α and auxiliary coefficient β for the new proposal

Table 6 : Accuracy of the new proposals (based on $f_{2,\theta}$), EN 1993-1-2 [1] and Lopes et al. [2] relative to the FE results for the flexural buckling assessment of stainless steel columns in fire

Table 7 : Assessment of the reliability of the new proposal (based on $f_{2,\theta}$), EN 1993-1-2 [1] and Lopes et al. [2] on the basis of the three reliability criteria set out by Kruppa [40]. Note that the numbers denoted by * violates the corresponding criterion.

Table 8 : Calibrated values of imperfection factor α , auxiliary coefficient β and plateau slenderness $\bar{\lambda}_{\theta,0}$ for the alternative method adopting the elevated temperature strength at 0.2% proof strength $f_{p0.2,\theta}$

Table 1: Comparison between critical temperature values θ_{cr} obtained through experiments [4, 8, 20] and finite element models for stainless steel columns in fire

Reference	Cross-section	End conditions	$L(\text{m})$	N_{Ed} (kN)	$\theta_{cr,test}$ (°C)	$\theta_{cr,FE}$ (°C)	$\theta_{cr,FE} / \theta_{cr,test}$
Gardner and Baddoo [4]	150×100×6	Fixed	3.40	268	801	722	0.90
	150×75×6	Fixed	3.40	140	883	791	0.90
	100×75×6	Fixed	3.40	156	806	747	0.93
	100×100×4	Pinned	3.99	80	835	736	0.88
	200×200×4	Pinned	3.99	230	820	714	0.87
Ala-Outinen and Oksanen [20]	40×40×4 (T1)	Pinned	0.89	44.6	873	803	0.92
	40×40×4 (T2)	Pinned	0.89	129.4	579	415	0.72
	40×40×4 (T3)	Pinned	0.89	114.4	649	565	0.87
	40×40×4 (T4)	Pinned	0.89	94.6	710	606	0.85
	40×40×4 (T5)	Pinned	0.89	54.8	832	774	0.93
	40×40×4 (T7)	Pinned	0.89	74.7	766	719	0.94
Tondini et al. [8]	80×80×3 (C1)	Fixed	3.00	72	709	742	1.05
	80×80×3 (C2)	Fixed	2.50	78	708	730	1.03
	120×80×3 (C3)	Fixed	2.50	100	705	740	1.05
Average							0.92
COV							0.095

Table 2: Comparison of load carrying capacities of simply-supported HEA 100 carbon steel columns in fire determined by Pauli et al. [27] $N_{u,test}$ and finite element models created in this paper $N_{u,FE}$

Test	Specimen	Buckling axis	$L(m)$	θ (°C)	$N_{u,test}$ (kN)	$N_{u,FE}$ (kN)	$N_{u,FE} / N_{u,test}$
HEA100_M_20C_z0	M01	z-z	0.85	20	857	803	0.94
HEA100_M_400C_z0	M02	z-z	0.85	400	646	588	0.91
HEA100_M_550C_z0	M03	z-z	0.85	550	405	351	0.87
HEA100_SL_20C_y0	L04	y-y	1.84	20	914	836	0.91
HEA100_SL_20C_y0	L15	y-y	1.84	20	859	836	0.97
HEA100_SL_20C_z0	L13	z-z	1.84	20	671	604	0.90
HEA100_SL_20C_z0	L10	z-z	1.84	20	512	604	1.18
HEA100_SL_400C_y0	L08	y-y	1.84	400	608	543	0.89
HEA100_SL_400C_z0	L16	z-z	1.84	400	466	373	0.80
HEA100_SL_550C_y0	L07	y-y	1.84	550	395	335	0.85
HEA100_SL_550C_z0	L11	z-z	1.84	550	297	239	0.80
HEA100_SL_700C_y0	L01	y-y	1.84	700	152	139	0.91
HEA100_SL_700C_z0	L12	z-z	1.84	700	128	109	0.85
Average							0.91
COV							0.106

Table 3: Range of the proportions of the cross-sections considered in the calibration

	h/b	b/t_f	h/t_w
Maximum	2.00	28.57	42.25
Minimum	0.93	5.30	10.00

Table 4: Summary of the parameters considered in the numerical studies used for the development and assessment of the stainless steel column fire design method put forward in this paper

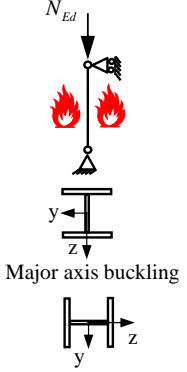
Loading condition	Cross-section			Stainless steel grades	Temperature	Slenderness $\bar{\lambda}_\theta$
	Austenitic	Duplex	Ferritic			
 <p>Major axis buckling</p> <p>Minor axis buckling</p>	HEM 100	HEM 100	HEM 100	Austenitic Duplex Ferritic	20 °C 200 °C 400 °C 600 °C 800 °C	0.2
	HEB 200	HEB 300	HEB 200			0.4
	HEAA200	HEA 300	HEAA180			0.6
	HEAA300	IPE 80	HEAA300			0.8
	IPE 100	IPE 100	IPE 100			1.0
	IPE 200	IPE 180	IPE 180			1.2
	IPE 300	IPE 180	IPE 300			1.4
						1.6
						1.8
						2.0

Table 5: Calibrated values of imperfection factor α and auxiliary coefficient β for the new proposal

Axis of buckling	Austenitic		Duplex		Ferritic	
	α	β	α	β	α	β
Major	0.90	1.00	0.55	1.00	0.55	1.00
Minor	0.90	1.50	0.55	1.50	0.55	1.50

Table 6: Accuracy of the new proposals (based on $f_{2,\theta}$), EN 1993-1-2 [1] and Lopes et al. [2] relative to the FE results for the flexural buckling assessment of stainless steel columns in fire

	Grade	N	Major axis buckling				Minor axis buckling			
			ϵ_{av}	ϵ_{COV}	ϵ_{max}	ϵ_{min}	ϵ_{av}	ϵ_{COV}	ϵ_{max}	ϵ_{min}
New proposals	Austenitic	770	1.17	0.080	1.41	0.88	1.16	0.079	1.42	0.94
	Duplex	660	1.12	0.075	1.33	0.91	1.17	0.127	1.51	0.92
	Ferritic	770	1.10	0.065	1.27	0.90	1.16	0.126	1.47	0.87
EN 1993-1-2 [1]	Austenitic	770	0.98	0.105	1.23	0.77	0.87	0.151	1.20	0.64
	Duplex	660	1.00	0.125	1.40	0.74	0.91	0.173	1.26	0.57
	Ferritic	770	1.10	0.156	1.76	0.78	1.00	0.148	1.74	0.65
Lopes et al. [2]	Austenitic	770	1.41	0.115	1.90	1.03	1.34	0.089	1.67	1.05
	Duplex	660	1.19	0.068	1.49	0.98	1.22	0.108	1.53	0.99
	Ferritic	770	1.56	0.135	2.21	1.09	1.54	0.133	1.82	1.06

Table 7: Assessment of the reliability of the new proposal (based on $f_{2,\theta}$), EN 1993-1-2 [1] and Lopes et al. [2] on the basis of the three reliability criteria set out by Kruppa [40]. Note that the numbers denoted by * violates the corresponding criterion.

	Grade	Major axis buckling			Minor axis buckling		
		Crit. 1	Crit. 2	Crit. 3	Crit. 1	Crit. 2	Crit. 3
New Proposals	Austenitic	0.00	3.90	-13.63	0.00	2.41	-13.27
	Duplex	0.00	8.18	-10.46	0.00	16.18	-13.25
	Ferritic	0.00	10.94	-8.35	0.00	12.50	-12.80
EN 1993-1-2 [1]	Austenitic	16.06*	56.97*	3.24*	56.15*	80.21*	16.87*
	Duplex	15.76*	45.76*	1.84*	35.60*	73.14*	14.32*
	Ferritic	4.56*	27.96*	-5.72	8.33*	52.50*	1.56*
Lopes et al. [2]	Austenitic	0.00	0.00	-28.22	0.00	0.00	-24.98
	Duplex	0.00	1.21	-15.89	0.00	1.29	-17.35
	Ferritic	0.00	0.00	-34.70	0.00	0.00	-33.86

Table 8: Calibrated values of imperfection factor α , auxiliary coefficient β and plateau slenderness $\bar{\lambda}_{\theta,0}$ for the alternative method adopting the elevated temperature strength at 0.2% proof strength $f_{p0.2,\theta}$

Axis of buckling	Austenitic			Duplex			Ferritic		
	α	β	$\bar{\lambda}_{\theta,0}$	α	β	$\bar{\lambda}_{\theta,0}$	α	β	$\bar{\lambda}_{\theta,0}$
Major	0.45	1.20	0.20	0.35	1.20	0.20	0.35	1.20	0.20
Minor	0.75	1.20	0.20	0.55	1.20	0.20	0.55	1.20	0.20